TAMPERE UNIVERSITY OF TECHNOLOGY

NOORA TUOVINEN

APPLICATION OF MAGNET QUENCH ANALYSIS

Master of Science Thesis

Examiner: Professor Hannu Eskola
Examiner and topic approved in the council meeting of the Faculty of Computing and Electrical Engineering on 12 January 2011

ABSTRACT

TAMPERE UNIVERSITY OF TECHNOLOGY
Master's Degree Programme in Electrical Engineering
TUOVINEN, NOORA: Application of Magnet Quench Analysis
Master of Science Thesis, 73 pages
April 2011
Major: Biomedical Engineering
Examiner: Professor Hannu Eskola
Keywords: LabVIEW, magnets, quench, quench protection, superconductivity

Post Mortem Analysis is a software tool built for CERN for hardware commissioning and post mortem event analyzing for the LHC. Magnet Quench Analysis application is a part of the Post Mortem Analysis tool and serves a base for analyzing quench data. It gives a possibility to observe and analyse data collected by the quench protection system.

The goal of this work is to study physics phenomena of superconductivity. Quench, quench protection and post quench data are studied in more detail. In addition, it describes how the existing LHC magnet quench analysis was extended to the new Quench Protection System data.

Based on the observations from magnet quench analysis, users can determine such parameters as firing times of the triggers and proper operation of the quench protection system. Application was developed using LabVIEW programming language. In this work especially quench detection, energy, location, heater protection and time delays are discussed.

It was discovered that automatic quench analysis saves precious time and reduces the need for manual calculations. Biggest problems during the project were found in code modification phase between different LabVIEW versions and programmers.

It is possible that further development of the code enhances the possibilities of quench analysis application. Designed methods for dipole magnets can be easily extended for different magnet types such as quadrupoles with changes in the configuration settings.

TIIVISTELMÄ

TAMPEREEN TEKNILLINEN YLIOPISTO
Sähkötekniikan koulutusohjelma
TUOVINEN, NOORA: Application of Magnet Quench Analysis
Diplomityö, 73 sivua
Huhtikuu 2011
Pääaine: Lääketieteellinen tekniikka
Tarkastaja: Professori Hannu Eskola
Avainsanat: LabVIEW, magneetit, karkaisu (quench), karkaisun suojaus, suprajohtavuus

Post Mortem Analysis on ohjelmistotyökalu, joka on ohjelmoitu CERN:lle LHC-laitteiston käyttöönottoa ja Post Mortem -tapahtumien analysointia varten. Magnet Quench Analysis -sovellus on osa Post Mortem Analysis -työkalua ja palvelee perustana karkaisun aikana syntyneen aineiston tulkinnassa. Sovelluksen avulla on mahdollista tarkkailla ja tutkia aineistoa, joka on kerätty suojausjärjestelmältä karkaisun yhteydessä. Tämän työn tarkoituksena on tutkia suprajohtavuutta fysiikan ilmiönä. Karkaisuun, karkaisulta suojautumiseen ja karkaisun aikana kerätyn aineiston tutkimiseen paneudutaan tarkemmin. Lisäksi työ kuvaa miten olemassa oleva LHC Magnet Quench Analysis -sovellus laajennettiin käyttämään uuden suojausjärjestelmän mukaista aineistoa.

Magnet Quench Analyysistä saatujen havaintojen perusteella, käyttäjät voivat määrittää muun muassa sellaisia tunnussuureita kuin liipaisuajat ja karkaisusuojausjärjestelmän kunnollinen toiminta. Sovellus on kehitetty käyttäen LabVIEW-ohjelmointikieltä. Tässä työssä kiinnitetään erityistä huomiota karkaisun havaitsemiseen, energiaan, sijaintiin, lämmitinsuojaukseen ja aikaviiveisiin.

Huomattiin, että automaattinen karkaisuanalyysi säästää arvokasta aikaa ja vähentää käsin tehtävien laskutoimitusten tarvetta. Projektin aikana havainnoidut suurimmat ongelmat ilmaantuivat lähinnä ohjelmointivaiheessa eri LabVIEW -versioiden ja ohjelmoijien välillä.

On mahdollista, että koodia edelleen kehittämällä voidaan parantaa uuden sovelluksen analyysimahdollisuuksia. Dipolimagneettien analyysivaiheet voidaan helposti laajentaa erilaisille magneettityypeille, kuten quadrupoleille, tekemällä muutoksia konfigurointiasetuksissa.

PREFACE

This master thesis was done at European Organization for Nuclear Research (CERN) for Measurement, Test and Analysis section of the Industrial Controls and Electronics group in the Engineering Department.

I would like to thank, first of all, professor Hannu Eskola at Tampere University of Technology for supervising my thesis.

My whole work section at CERN also deserves thanks. Special thanks for my section leader Adriaan Rijllart and my supervisor Hubert Reymond. I am grateful to them for giving me this exceptional and inspiring opportunity at CERN. I am thankfull for all the support they gave me throughout the project. In addition, I would like to thank my office mates Dmitriy Kudryavtsev and Cedric Charrondiere for unforgettable atmosphere at the office.

I would also like to thank my family and friends. Special thanks for my very best friends Saija Hopea and Hanna Rask for being there whenever needed. Thanks for my house mate in France Donat Holzer for reading through various versions of my thesis. Thanks to my sister Petra for all the inspiration and mum who never forgot to ask me about my graduation date. Thanks to everyone whose names are not mentioned here and who have helped throughout my years of studies.

Without a doubt, my boyfriend Hayes Brien deserves thanks. He always supports me and will not let me give up which has helped me in reaching this goal.

Tampere, 1st of March 2011

Noora Tuovinen

CONTENTS

PARAMETERS

B_c	Critical magnetic field
H_c	Magnetic field strength
H_{c1}	Lower magnetic field strength
H_{c2}	Higher magnetic field strength
I_MEAS	Current Measurement (*kA*) at 50 *Hz*
I_REF	I_REF is the current reference (*kA*) at 50 *Hz*
J_c	Critical current
T_c	Critical temperature
Td	Quench detection time from U_QS0=100 *mV*
tDump	Time from U_DUMP_RES=100 *V*
tFire	Heater firing time from U_HDS
Tmax	Hot spot temperature
tTrigger	Trigger time from I_REF=0 *A*
Tq	Programmatically determined actual quench beginning
Tq_v	Visually determined actual quench beginning
U_1	Voltage across external aperture
U_2	Voltage across internal aperture
U_HDS	Quench heater voltage
U_QS0	Voltage difference U2-U1

ABBREVIATIONS

AD	Antiproton Decelerator
ALICE	A Large Ion Collider Experiment
AQA	Automatic Quench Analysis
ATLAS	A Toroidal LHC ApparatuS
CERN	Conseil Européen pour la Recherche Nucléaire (European Organization for Nuclear Research)
CMS	Compact Muon Solenoid Experiment
CNGS	CERN Neutrinos to Gran Sasso
CTF3	Clic Test Facility
FCL	Fault current limiter
FGC	Function Generator/Controller folders
HTS	High Temperature Superconductor
ISOLDE	Isotope Separator OnLine Device
LabVIEW	Laboratory Virtual Instrument Engineering Workbench
LEIR	Low Energy Ion Ring
LFMRI	Low-field magnetic resonance imaging
LHC	Large Hadron Collider

LHCb	Large Hadron Collider Beauty Experiment
LINAC	Linear Accelerator
LTS	Low Temperature Superconductor
MB	Dipole magnets to deflect the beam
MCG/MKG	Magnetocardiography
MEG	Magnetoencephalography
MENG	Magnetoenterography
MGG	Magnetogastrography
MHD	Magnetohydrodynamics
MIITs	Measure of dissipated energy during a quench
MNG	Magnetoneurography
MQ	Twin-aperture main quadrupole magnets in the arcs
MRI	Magnetic Resonance Imaging
n-ToF	Neutrons Time Of Flight
NbTi	Niobium-titanium, widely used superconductor
PM	Post Mortem system
PS	Proton Synchrotron
PSB	PS Booster
QPS	Quench Protection System
SDDS	Self Described Data Set file format
SM18	Magnet test facility for dipole testing
SMES	Superconducting magnetic energy storages
SPS	Super Proton Synchrotron
SQUID	Superconducting QUantum Interference Device
VI	Virtual Instrument, LabVIEW program or subroutine imitating real instruments

1. INTRODUCTION

In the search for Higgs boson (to complete the Standard Model), nature for dark matter (accounts for 26% of the mass of the universe), signatures of supersymmetry and other puzzling questions of the universe, scientists have built world's largest and most powerful particle accelerator. Known as the Large Hadron Collider or briefly the LHC it enables scientists to study the smallest known particles in the universe. Such research programs as the LHC stimulate new innovations and pilot applications on various fields including medical applications.

The LHC uses superconductive magnets in the accelerator ring to provide a strong magnetic field. This enables the beams to be guided around the accelerator ring. Despite the advantages in the use of superconductive magnets there are some problems rising during operation such as quench. Analyzing quench process is an important parameter in understanding the machine and magnet operation. Especially from the point of view of quench protection, being able to detect quench reliably is of great importance. A quench protection system has been implemented to the LHC and in case of beam loss or quench, a specific tool to collect all the information from the various sub-systems is in use. This tool is called Post Mortem and can be used to analyze the data.

The goal of this thesis is to study physics phenomena of superconductivity and quench focusing on analysis, especially the actual quench event. First, the theory behind superconductivity is discussed. After this, the quench process and protection possibilities are introduced. Designing methods are discussed to give a good general view of the procedures needed to meet the goal. Explanations how the application helps experts analyzing quench and how it can improve the performance of the LHC are given. Hereafter, results given by the new quench analysis are studied in more a specific way giving emphasis to the detection of quench triggering times. In the conclusion, the future and possibilities of superconductivity and designed quench analysis are discussed.

This thesis is related to the LHC project at European Organization for Nuclear Research (CERN). It was done for Measurement, Test and Analysis section of the Industrial Controls and Electronics group in the Engineering Department and acts as a part of the Post Mortem Analysis tool.

2. SUPERCONDUCTIVITY

2.1. Basic Principles

Superconductivity is a physics phenomenon which allows some metals to lose their resistivity and become perfect conductors when cooled down to very low temperatures (normally ranging between -272 and 253 *ºC* (1 and 20 *K*). Solid mercury, for example, has limit temperature of -268.8 *ºC* (4.2 *K).* When cooled under metals characteristic critical temperature, resistance is absolutely zero. The critical temperatures for metals are normally very low but scientist are studying to find materials with even higher critical temperature superconductors and have managed to find a material with as high a critical temperature as -19 *ºC* [Superconductors.org]. Zero resistivity is very advantageous for different applications of which examples are given later. Figure 2.1 shows a graph for the resistivity and how it drops to zero below critical temperature in the case of mercury, which was the first superconductor found.

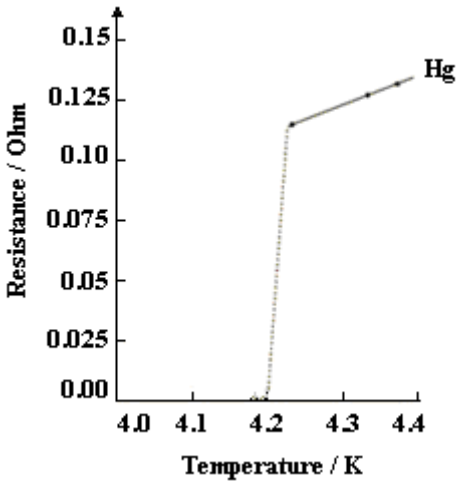

Figure 2.1 Resistance on Mercury

Superconductors can be classified upon different criteria and one of these is their critical temperature. Low temperature superconductors (LTS) are materials which are superconductive only at very low temperatures. Niobium-titanium (NbTi) which is used in the LHC and largely in other applications is an example of LTS material. It has a critical temperature of -263.6 *ºC* (9.4 *K).* High temperature superconductors (HTS) have higher critical temperatures. There is no exact critical temperature value for the change from LTS to HTS materials but all the compounds, which are superconductive above -196 *º C (77 K),* are considered as HTS materials.

Classifying with physical properties gives type I and II superconductors as shown in Figure 2.2. Type I includes mostly elemental superconductors but also few alloy superconductors. These kinds of superconductors are homogeneously in superconductive state, apart from the very topmost coating. Their superconductive regions resist magnetic fields; this is called the Meissner effect. It only happens if the magnetic field is not too high. Type I superconductors have only one critical magnetic field strength value Hc.

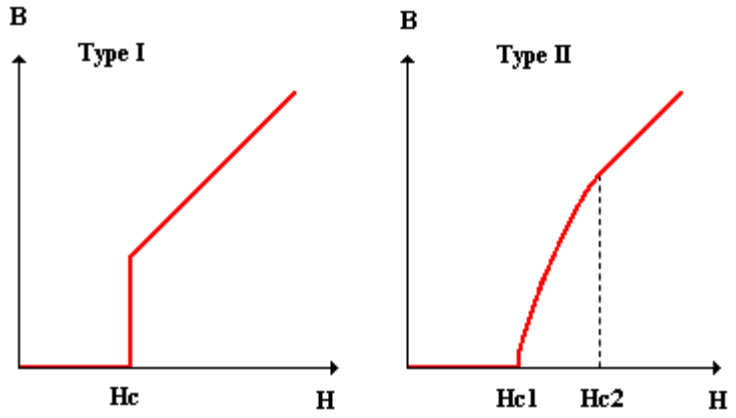

Figure 2.2 Differences between type I and II Superconductors

Most of the superconductors are type II superconductors and they are typically alloys. The material is a mixture of normal and superconductive state regions as a vortex structure. Type II superconductors have two critical magnetic field strength Hc values. Below Hc1, type II materials are superconductive, and above Hc2, they become resistive. In between Hc1 and Hc2, the resistivity is zero but magnetic field can penetrate inside the material through the normal regions and this creates turbulent currents to the superconductive regions; this is a mixed state Meissner effect. Type II superconductors remain superconductive to much higher fields. [FYS-1500, Mess et al. 1996, Wilson 1983]

2.2. Applications

Superconductivity finds many applications and a closer look on biomedical and collider applications is taken with the examples from Magnetic Resonance Imaging (MRI), Superconducting Quantum Interference Device (SQUID) and the Large Hadron Collider (LHC). In general, commercial applications are quite rare since the cooling of superconductors is quite expensive and materials are complex. Figure 2.3 shows the global market for superconductivity, as seen in December 2009, by Consortium of European Companies determined to use superconductivity (Conectus). It is obvious from the diagram that MRI is the most widely used application of superconductivity. The figure shows that superconductivity will keep on evolving, and that HTS material will become more and more important in the future. Superconductive materials are very interesting because they allow saving of energy, and products made from them are

normally 50 % smaller and lighter. Also, environmentally their manufacturing process does not create as much greenhouse gases as manufacturing of conventional components.

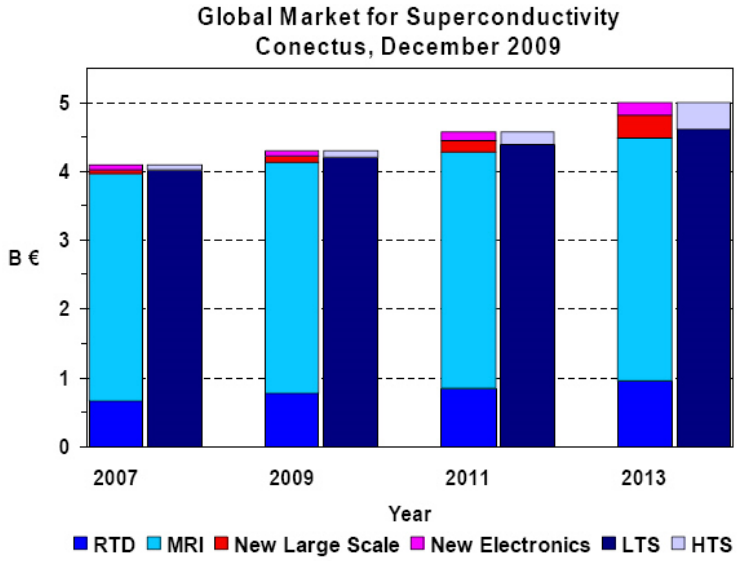

Figure 2.3 Global Market for Superconductivity, [Conectus]

Superconductor applications on electrical field include superconducting colliders, electric superconducting generators, synchronous motors and transformers. Network applications include, for example, fault current limiters (FCLs), superconducting magnetic energy storages (SMESs), transmission of commercial power and flywheels with HTS bearings. Other applications, such as magnetic-levitation transport vehicles (trains etc.), petaflop computers, nuclear fusion, magnetic separation (for treating waste waters which contain heavy metals), magnetic force control (in drug delivery systems) and magnetohydrodynamics (MHD) are also interesting. Superconductivity also finds military uses such as degaussing ship's hull, antennas and electromagnetic pulse to disable enemy's electronic equipment. [Della Corte 2009, Hartikainen 2003, Superconductors.org]

2.3. Biomedical Applications

Superconductivity finds many uses in the biomedical field. MRI uses superconducting magnets to attain high treatment fields and they may also be used in ultrasound and magnetic surgery. Another application of superconductivity is Superconducting Quantum Interference Device (SQUID) for biomagnetic measurements. It has an advantage of detecting very small magnetic fields in the field area of microteslas. Many of the applications in medicine are used only in research and are not yet commercially implemented.

2.3.1. Magnetic Resonance Imaging

By far, the leading commercial application of superconductivity is found in the biomedical field. Magnetic resonance imaging (MRI) is a noninvasive diagnostic tool which was first used on a human in July 1977. MRI is quite a new imaging method and in Finland the first machine was used in 1984. [Jokela et al. 2009, Magnet Lab 2010]

In clinical use, MRI's are used with static magnetic fields between 0.2-3 *T*. Open MRIs are also sometimes used, but they only allow fields up to ~1 *T*. Open MRIs find advantages in use for example in the case of claustrophobic or overweight patients. They also allow surgeons to operate whilst imaging. Demand for higher fields for MRI is on going all the time. In research, as high fields as 9.4 *T* are used for whole-body MRI. Only four machines allowing high field like this exist. In addition, use of a whole-body MRI of 11.7 *T* at Neurospin is scheduled for end of 2012. This field is told to be the physical limit at which it is possible to use established technologies for MRI machines, such as cooling of the coils. Higher fields have advantages in image quality IQ due to higher signal-to-noise ratio, SNR and enhanced resolution. Anyhow, they require high uniformity magnets and temporal stability. Use of higher fields allows new applications to be introduced. [EuH 2009, Jokela et al. 2009, Lvovsky & Jarvis 2005, Magnet Lab 2010, Wired.com]

With MRI it is possible to get 2D and 3D images of human body at any orientation and depth. The method is based on the nuclear magnetic properties of hydrogen nuclei in the body tissues. Human body consists of around 63 % of water and fat. MRI uses 3 different magnetic fields in its operation. A strong static magnetic field between 0.6-3 *T* is always present in the tube. During the operation small gradients are applied with change rate around 20 *mT/ms* and pulsative radiofrequency fields between 10–128 *MHz*. [Jokela et al. 2009, Lvovsky & Jarvis 2005, Magnet Lab 2010]

MRI's are used to image variety of structures in the human body. With low fields, one can image for example lungs or wrists, and with higher fields and thus better image quality such structures as nervous systems can be imaged. Development of MRI machines has given possibilities also for imaging vascular systems and doing functional investigations. MRIs are good for example for brain, spinal, cardiac or joint imaging. [Jokela et al. 2009]

The future of MRI relies heavily on higher magnetic fields. Machines now used in research will most likely become clinical practice at some point. The obstacle in the way for clinically implementing higher fields is its unknown impacts on health. However, using high field MRIs bring better image quality with even lower operation time. Designing for advanced magnetic, cryogenic and integrated system is on-going. Challenge for the future is also the HTS materials. Their mechanical properties bring difficulties for the design and it is also hard to design sufficient quench protection. However, their potential is high, and it might be possible to use fields as high as 20 *T*. In addition, dimensional accuracy and consistency of I_c over long piece lengths for HTS materials are hard to keep. Furthermore, absence of effective persistent joint technology

brings difficulties for their design. However, HTS MRI unit designs do exist. With higher operating temperatures it is possible to get high conductor stability due to increased enthalpy margin. [Gourlay 2008, Lvovsky & Jarvis 2005, Magnet Lab 2010]

If accelerator magnets such as the LHC and superconductive magnets for medicine are compared, it is seen that drive for using them is a bit different. While the LHC is trying to find answers for physics theories, the aim of MRI is to study and cure human body. MRI designs are made in a competitive environment where few publications and technical information are widely available. As a result, different MRI machines find different approaches to achieve the same goal. Designs are often driven by the cost with the desire for optimized installation and calibration to attain minimum service for the machines later on. [Lvovsky & Jarvis 2005]

In the case of a quench (see Chapter 3), during the use of MRI, not much information is publicly available, probably due to the competitive environment. What is said is that quench event is very unlikely, since MRI machines are basically designed to be quench-free. They have a huge reliability and stability since quench is also a matter of patient safety. They are fully self-protected and a monitoring system is checking constantly for abnormal situations. Helium level is monitored and magnets are equipped with an emergency system. MRI magnets have been designed to direct gaseous helium directly outdoors through a quench pipe to avoid harmfulness to people inside. Without this design, helium would eventually displace room air and leave patients without oxygen. There also exists a risk of hypothermia and cold burns since released helium (or liquid nitrogen) is very cold. Specific quench codes and design solutions have been implemented to minimize high voltage and temperature. [Lvovsky & Jarvis 2005]

Treating with high (or low) magnetic fields might produce some health effects. If the magnetic field goes above 4 T it is considered to create some health effect such as dizziness, nausea, increase of blood pressure and arrhythmia. Static magnetic field may also interfere with electronic implants such as pacemakers or defibrillators. In addition, problems occur with metallic parts within the body which may heat up the tissues or start moving in the result of being in magnetic field. [Allison, GE, Hitachi, Jokela et al. 2009, Servomaa & Parviainen 2001, Siemens, Varian]

2.3.2. Superconducting Quantum Interference Device

Superconducting quantum interference devices allow detecting of very small magnetic fields non-invasively. SQUIDs can be used in a variety of biomagnetism applications, for example in magnetoencephalography (MEG) for brain, magnetocardiography (MCG) for heart, magnetoneurography (MNG) for neural system, magnetoenterography (MENG) for intestines, magnetopneumography for lungs, liver iron susceptometry, magnetogastrography (MGG) for stomach, immunoassay in vivo for breast cancer and low-field magnetic resonance imaging (LFMRI). Low-field MRIs are used instead of High field MRIs, because of cost reductions and better access. Anyhow, LFMRIs have a bad signal-to noise and spatial resolution in comparison to high field MRIs.

SQUIDs combine two phenomena of the superconducting state: Josephson tunneling and flux quantization. They use two Josephson junctions connected in a parallel superconducting loop. Changes in magnetic flux are measured through a pick-up loop, and even small differences produce change in voltage. One reason to use SQUIDS is that biological signals are at low frequencies below 50 *Hz*, and only SQUIDS have enough sensitivity to detect them. [Clarke et al. 2007, LANL, McDermott et al. 2004]

2.4. Large Hadron Collider

The Large Hadron Collider (LHC) is a 26.7-kilometer long accelerator ring situated at CERN, near Geneva in Switzerland. The LHC stretches to both sides of the border of France and Switzerland. It is the biggest scientific instrument ever built and lies about 100 metres underground. The LHC is designed for colliding proton beams of 7 *TeV* and heavy ions, such as lead, at 2.8 *TeV/amu* with two beams counter-circulating in the accelerator ring. With the help of the LHC and its experiments, scientists study the smallest known particles hoping to find answers related to dark energy, dark matter, extra dimensions, Higgs boson and supersymmetry.

The travel of protons towards collisions starts from the linear accelerator, after which they are injected into the PS Booster. After this, they go through the Proton Synchrotron (PS) followed by the Super Proton Synchrotron (SPS). Finally, the particle beams with low energies reach the LHC. In this point, the field of the main dipoles is 0.54 T. During the next 20 minutes, beams are circulated gaining more energy with every round while the field in the main dipoles is increased up to 8.3 T. Eventually protons reach very high energies and almost the speed of light before they are collided to each other. Beams are focused with the help of special quadrupoles. This goes on for another 2 to 10 hours before the beams are dumped. The field in the dipole magnets is decreased back to 0.54 *T* and is kept there for the next 20 to 40 minutes. After this, beam injection can be repeated with the ramping of the field back up to 8.3 *T*. Figure 2.4 shows the whole accelerator complex of the LHC. [Rossi 2009]

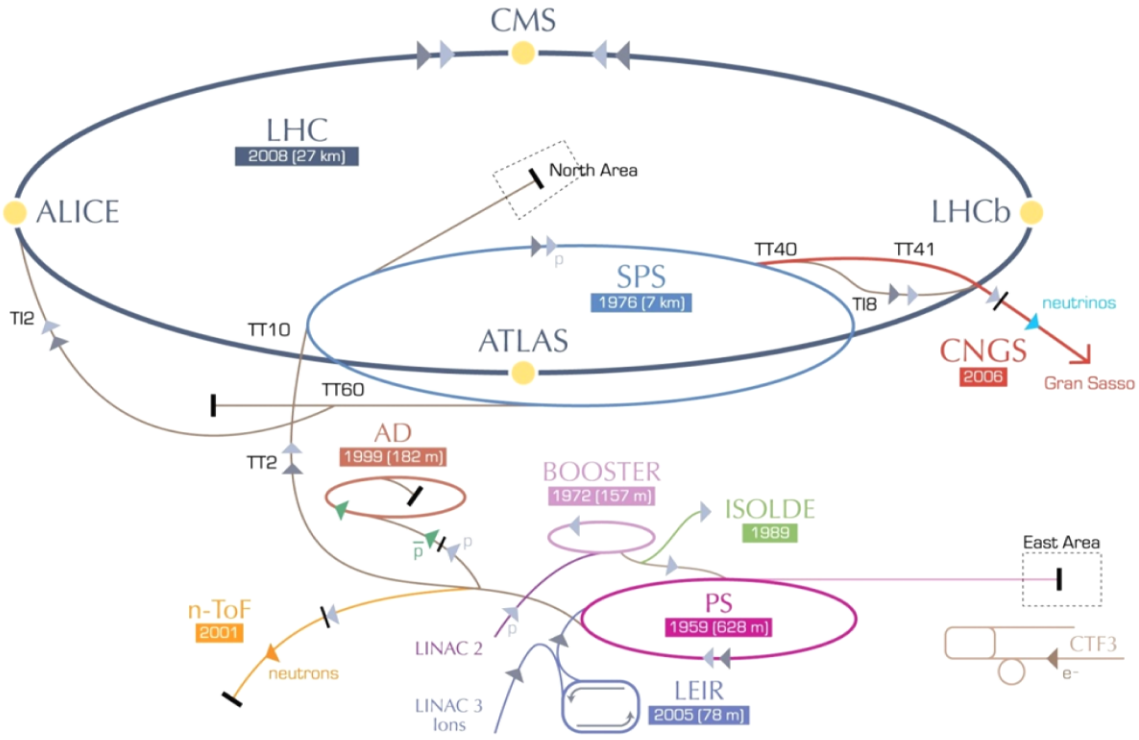

Figure 2.4 CERN Accelerator Complex. Explanations:AD Antiproton Decelerator, CTF3 Clic Test Facility, CNGS CERN Neutrinos to Gran Sasso, ISOLDE Isotope Separator OnLine Device, LEIR Low Energy Ion Ring, LINAC Linear Accelerator, n-ToF Neutrons Time Of Flight. Source: CERN

The LHC takes advantage of superconductivity in its operation by using about 10 000 superconducting magnets. Superconductivity allows magnets in the LHC to have zero resistivity under certain conditions. They are built from niobium-titanium and cooled down to temperatures of -271 ^{o}C (1.9 K) by a huge cryogenics system. Because of the very low critical temperature of niobium-titanium, liquid helium needs to be used as a refrigerant. At low temperatures, it can reach all the smallest cavities thanks to superfluidity characteristics and is able to maintain the stability of the coil. Superconductivity allows magnetic fields up to 8 T to be reached without heat dissipation. Using superconductivity allows higher particle energies and can save operation costs of the machines but meets unique difficulties such as the quench, which is discussed in more detail later on.

The main experiments detect particles at the points where the beams are collided. The four main experiments are called ALICE (A Large Ion Collider Experiment), ATLAS (A Toroidal LHC ApparatuS), CMS (Compact Muon Solenoid Experiment) and LHCb (Large Hadron Collider Beauty Experiment). ATLAS and CMS use giant superconducting magnets to improve sensitivity. In addition, using superconductive magnets and the strong magnetic field they provide, one is able to guide the beams around the accelerator ring. All in all, the LHC uses 1734 large magnets and 7724 smaller size superconductor corrector magnets. The main magnets are the dipole magnets which deflect the beam and the quadrupole magnets which focus

the beam. There are 1232 twin-aperture dipole magnets of 15 *m* length in the LHC. Figure 2.5 shows the cross-section of a LHC dipole magnet. All magnets in the LHC store a significant amount of energy which can create intense damage in the case of fault in the operation. [CERN, Erokhin 2008, Rodriguez-Mateos 2001]

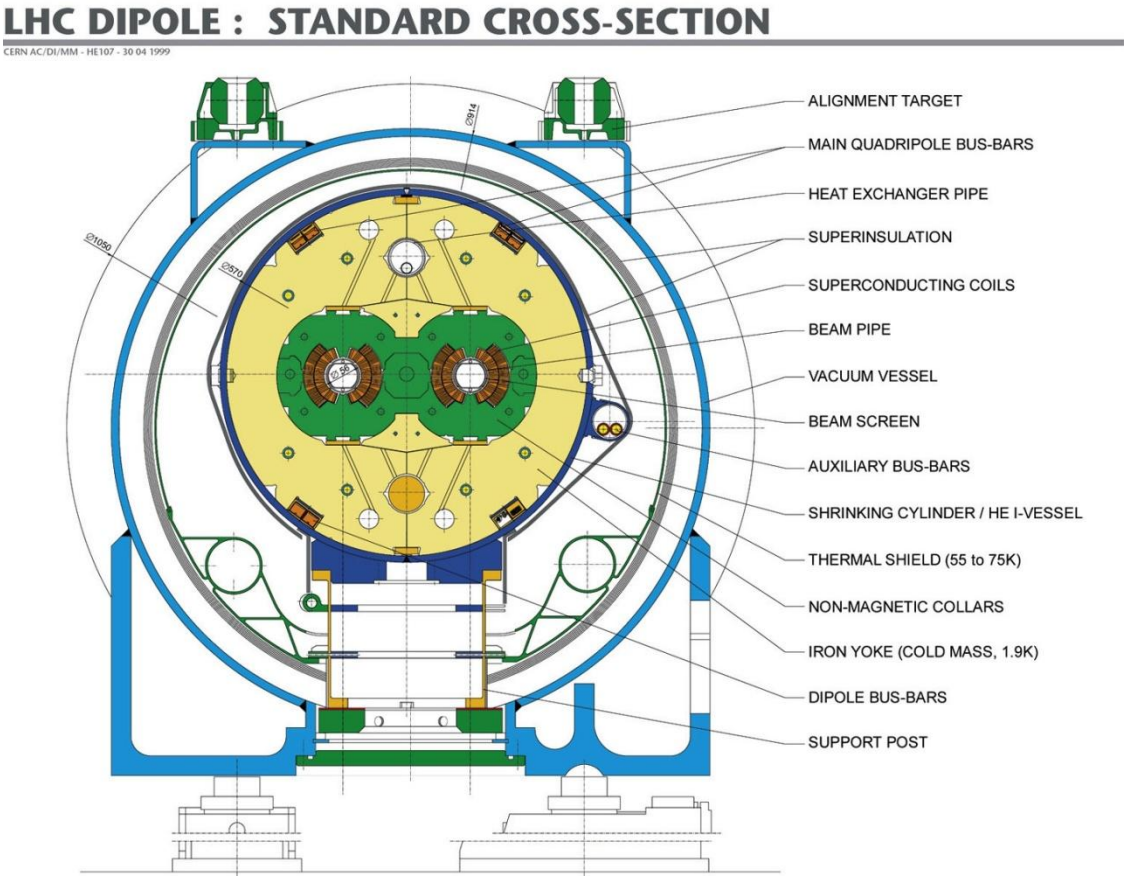

Figure 2.5 LHC Dipole Magnet Cross-section, source: CERN

The LHC is a culmination of twenty years of design and constructing with expert knowledge and co-operation between engineers, physicist and mechanics from all over the world. The LHC was began operation 10th of September 2008 but was soon followed by a quench incident 19th of September which forced a delay to the operation. The next run started on 20th November 2009 after repairs had been made. Since then, the LHC has been operated at 3.5 *TeV* per beam including some technical stops in between. On the 8th of November 2010, collision between lead ions was commenced at the LHC with the energy of 2.76 *TeV* per nucleon pair and continued until the end of the year 2010, and starting the new year of 2011 with proton-proton collisions. [CMS, PR15]

3. QUENCH

3.1. Introduction

A quench is a resistive transition from superconducting state to normal state. It should be avoided because it has a negative impact on the lifetime of a magnet. After a quench, coil needs up to two hours for recovery into superconducting state. All in all, it takes 30 minutes to 5 hours to restart the LHC after a quench [Yurkewicz 2007]. During this time, no beam can be injected and all this time is time off from experiments. Quench may and will happen in all superconducting magnets. This is especially true for accelerator magnets because of high current densities. Accelerator magnets have high current densities because the volume of an accelerator magnet is kept small. When current density is increased, the stability of the magnets decreases. In the case of the LHC, quenches can happen either in the main dipoles, the quadrupoles or the bus bars, and the circuits have to be protected against them. The bus bars are the connections between magnets. Different methods of quench protection are discussed in the later chapters mainly in the case of the LHC.

Quench propagates from one coil to the next by thermal conduction. The initial starting point forms the hot spot at temperature T_{max}, since it is the spot where quench has the most time to develop. The propagation happens with a quench propagation velocity. It happens either longitudinally (along the length of the superconducting wire) or transversally across the insulation layer as seen in the Figure 3.1.

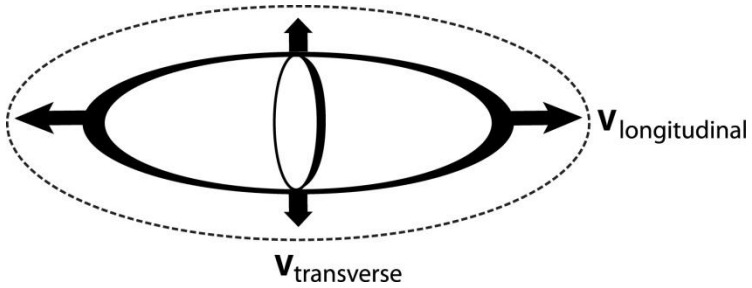

Figure 3.1 Quench Propagation

Transition from superconducting state to normal state happens in the case of exceeding critical value of either temperature, current or magnetic field. This is often referred as a three dimensional phase diagram called critical surface. In the case of the LHC magnets, the used superconductor material is niobium-titanium, and its critical surface is shown in Figure 3.2.

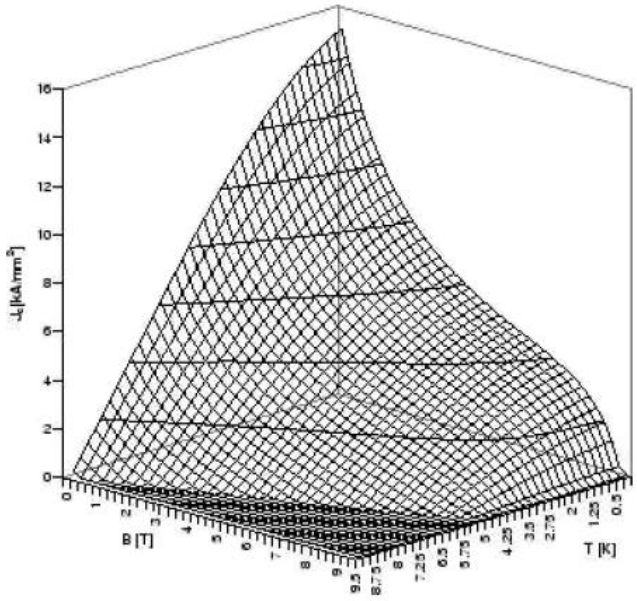

Figure 3.2 Critical Surface of Niobium-Titanium, Source [Motiwala & Sridhar]

The area under the surface is in a superconducting state and when any of the values lie above the critical surface, the material changes to normal state by quenching the magnet. Increase in any of the properties produces a decrease in the other two. The current density is normally constant throughout the coil. Critical values for niobium-titanium are for temperature T_c=9.4 *K* (when B=0 *T* and J=0 *A/mm*^{2}); for magnetic field B_c=14.5 *T* (at T=0 *K* and J=0 *A/mm*^{2}); and for current J_c=2.10^4 *A/mm*^{2} (at T=0 *K* and B=0 *T*). It is worth noting, that the temperature margin between conductor working temperature and the critical temperature is very small. For LHC dipoles this margin is around ~1.2-1.4 *ºC*. This is the reason why quenching can be generated by even small movements of local temperatures. [CAS 1996, Ferracin & Prestemon 2009, Motiwala & Sridhar, Quench-analysis]

3.2. Detection

Best quench protection, is to design magnets to hardly quench under normal operating conditions. Other than that, fast and reliable quench detection serves as a crucial element of quench protection. Any rise of the voltage across the magnet indicates that a quench has occurred and that certain procedures need performing. The rising voltage across the magnet is caused by the resistance. The current in the magnet changes very slowly because of the inductance. After the quench has been detected, the quench detection system triggers the firing of heaters in the magnet which is quenching. It also activates the extraction system, causing a decay of the current in the entire circuit with a time constant of about 95 *s.* Figure 3.3 shows a graph how quench is detected with the change of voltage. Pink and green graphs of U_1 and U_2 show voltages in different apertures of the magnet. U_2 is the voltage across internal aperture and U_1 is the voltage across external aperture. When one of them changes even with a slightest amount it is detected in U_QS0. U_QS0 is the difference between these two signals and

is amplified to show even the smallest changes. This is shown in U_QS0 having a visible change in curve before U_1 and U_2. The X scale in the graph is chosen so that zero point is the time when I_REF becomes 0 amperes, because of the nature of the used application. I_REF is the current reference (*kA*) at 50 *Hz*.

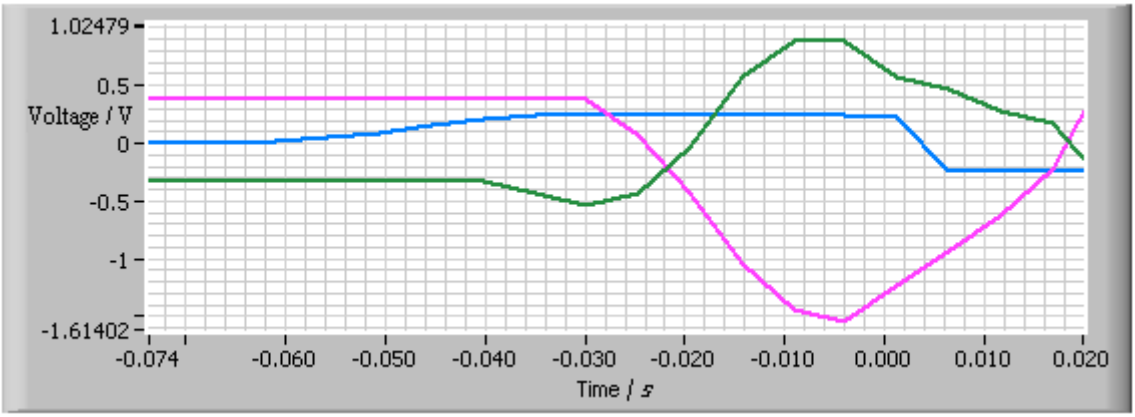

Figure 3.3 Quench Detection from U_QS0. Voltage across internal aperture U_1 is pink, voltage across external aperture U_2 is green, amplified difference between U_1 and U_2: U_QS0 is blue

There is a floating bridge detector for each magnet in the LHC circuit to detect quenches. Quench is detected when U_QS0 signal exceeds the threshold voltage of 100 *mV* and stays over this value for longer than 10 *ms*. Threshold voltage has been introduced because of noise in the voltage taps. The quench detection system triggers in few milliseconds a discharge of the heater power supplies of the quenching magnet. It also triggers simultaneously the opening of the two extraction systems and switches off the power converter.

After this, bypass thyristor ensures the circuit continuity. The current starts to decay and the start of the ramp down is visible in Figure 3.4 by the change in the slope. About 25 *ms* later, heat that has developed in the quench heaters causes transition to normal state, which can also be seen as a change in the slope. When the voltage over the entire magnet reaches 6 *V*, diode starts to conduct and the current in the quenching magnet commutes into the diode.

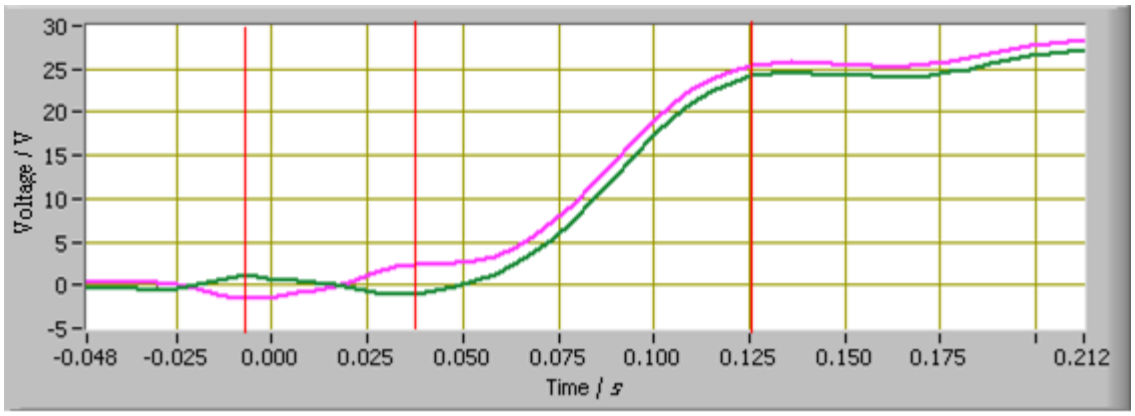

Figure 3.4 Quench. Voltage across internal aperture U_1 is pink, voltage across external aperture U_2 is green.

Quench Propagation happens longitudinally in to the non-heated sections with a velocity in the range of 15 *m/s* to 20 *m/s* for MB dipole magnets. Heat flow from the quenching magnet usually leads to secondary quenches of neighboring magnets which are situated in the same cell. At low currents propagating happens with faster velocity and this is sufficient to prevent overheating and other mal effects. [Ferracin & Prestemon 2009, Rodriguez-Mateos et al. 2000, Rodriguez-Mateos 2001, Siemko 2001, Verweij et al. 2008]

3.3. Different Types

Quenches may occur for a variety of reasons. *Training quenches* are done for gradual improvement of the magnet's performance. Training quenches make progressive increase of quench current possible and thus the magnet improves quench after quench. These kinds of premature quenches are due to conductor motions, epoxy resin cracking and micro yielding in the niobium-titanium. During the first quench, part of a winding starts to move. Next quench will happen in another part of the winding if the first part is in stable position and this enables higher current. Usually, it takes a few quenches of increasing currents to reach plateau of constant current.

Quench may also occur in cases other than training due to conductor motions. These kind of *mechanical disturbances* may happen if there are structural disturbances such as micro-fractures, cracks or just motions of structural elements. Accidental beam losses may induce quenches. *Beam induced quenches* should not occur in case of regular beam losses in the LHC since the system is designed to take them into account. However, accidental beam losses, such as malfunctioning of power supplies, kicker magnets and other components [Mess 1996], can deposit enough energy to induce a quench by exceeding the critical temperature. *Heater quenches* are provoked either for protection or for determining the minimum quench energy at a given current to study the quench propagation. *Cryogenic failure* is another possible reason for quench to occur. If the cryogenic system fails, temperature increases and provokes a quench. *Electrical sources* may also generate enough power i.e. heat for internal joule

dissipation. If the joule heating (I^2R losses) is sufficient, a region might reach the critical temperature. This may occur during ramping due to cable hysteresis loss, inter-strand coupling, inter-filament coupling, other eddy currents (spacers, collars) and resistive joint (splices). *Electric faults* such as false quench detection, false triggering and powering the coil above allowable current may provoke a quench too.

Symmetric quench may delay the quench detection and in that way endanger the circuit and the magnets. This kind of quench is shown in Figure 3.5.

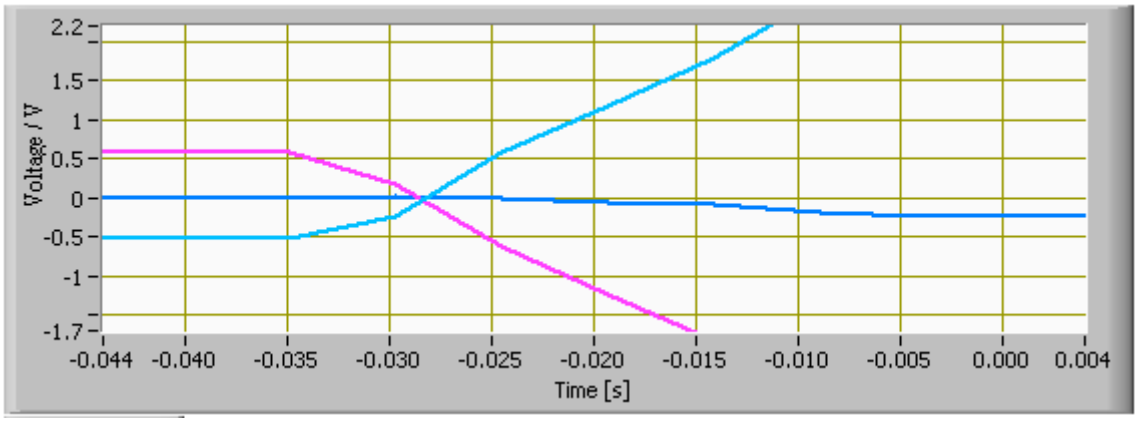

Figure 3.5 Symmetric Quench 23.5.08 at 7:44:16. Voltage across internal aperture U_1 is pink, voltage across external aperture U_2 is light blue,, amplified difference between U_1 and U_2: U_QS0 is blue

It is shown that both apertures U_1 and U_2 quench in an almost identical way. For this reason, the quench detection is delayed, since the change is not visible in even U_QS0. In the worst cases, quench may go unnoticed. This increases the temperature at the hot spot of the coil. Safe detection of symmetric quenches may be done by comparing voltage drops across magnets. [Bhunia 2003, Ferracin & Prestemon 2009, Kurfuerst, Mess et al. 1996, Rodriguez-Mateos 2001, Rodriguez-Mateos et al. 2000, Siemko 2001, Verweij et al. 2008]

3.4. Protection

3.4.1. Quench Effects

As mentioned earlier, a key requirement of quench protection is fast quench detection. Accelerator systems combine many techniques protecting the magnets reliably and quickly. Protection elements used within the LHC are discussed in the next sub-chapters. The quench protection system layout, which consists of individual quench detection systems, cold by-pass diodes, quench heaters and two independent extraction systems, is shown in Figure 3.6. Arrows show how the signals are measured.

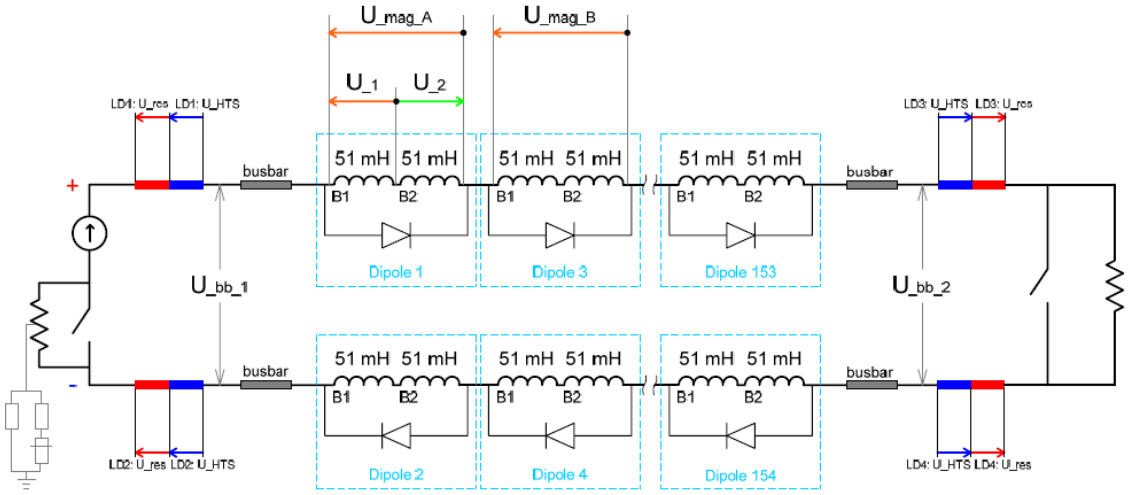

Figure 3.6 Quench Protection System for Dipole Magnet in the LHC, Source [Erokhin 2008]

In order to protect superconducting magnets in the case of a quench, the energy which is stored in the magnetic field has to be converted to heat. At high currents, quench may destroy the LHC magnets. Different kinds of damage that may occur due to overheating are, for example, insulation or conductor degradation and melting of the splices or conductor. High voltages then again cause arcing and short circuits. In addition, mechanical strains and faults due to overstressing might damage the magnets. Overstressing may cause large thermal expansion stresses and structural failures, strain-induced conductor damage, helium pressure and mass-flow-induced damage.

Quench protection systems are needed since the natural quench propagation would not be sufficient (fast enough) to protect the circuit. After the quench, stored magnetic energy has to be uniformly distributed to the coils. This can be done by firing the heater strips after the quench detection. Each of the eight sectors of the machine is powered independently to limit the amount of stored energy in the main electrical circuits. [Ferracin & Prestemon 2009, Rodriguez-Mateos et al. 2000, Rodriguez-Mateos 2001, Rossi 2009, Siemko 2001]

3.4.2. Quench Heaters

Quench heaters are used in the LHC as an active method of spreading the quench. This is not as reliable protection as passive methods but when used together with passive methods serves as a good base for protection. Stored energy is dumped into each of the quench heaters and is homogenously spread for all the magnets of the circuit. Heaters switch enough resistive volume for the energy to safely dissipate in the coils. This way, all the superconducting cables heat up and lose their superconductivity and become resistive. This resulting resistance distributes the energy of the magnet equally over all the cables and so keeps the maximum temperature and voltage in safe limits. An example of the quench heater voltage U_HDS behavior before and after the firing of the heaters is shown in Figure 3.7.

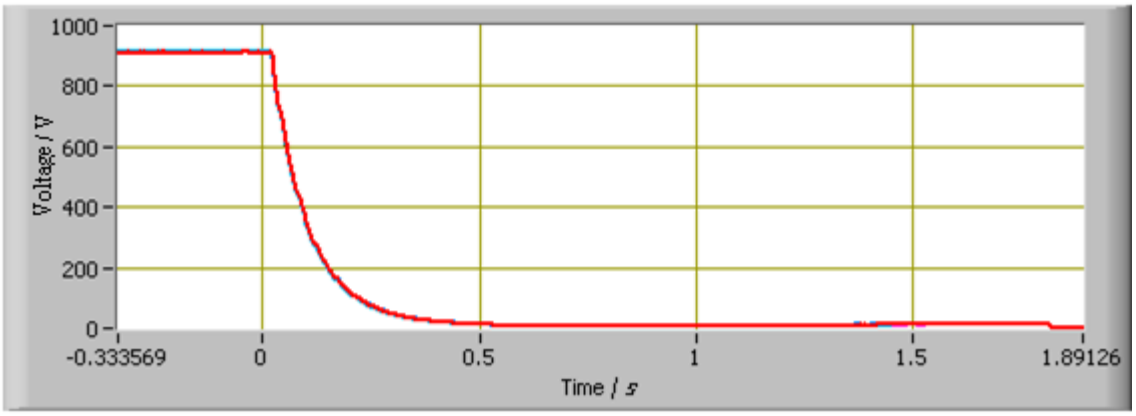

Figure 3.7 Quench Heater Voltage Signals During Quench

In practice, quench heaters of the LHC consist of pairs of stainless steel strips partially plated with copper. Copper is introduced to reduce their resistance and to allow connections of heater strips in series. The heater strips are bonded between two layers of polyimide electrical insulation foil (see Figure 3.8).

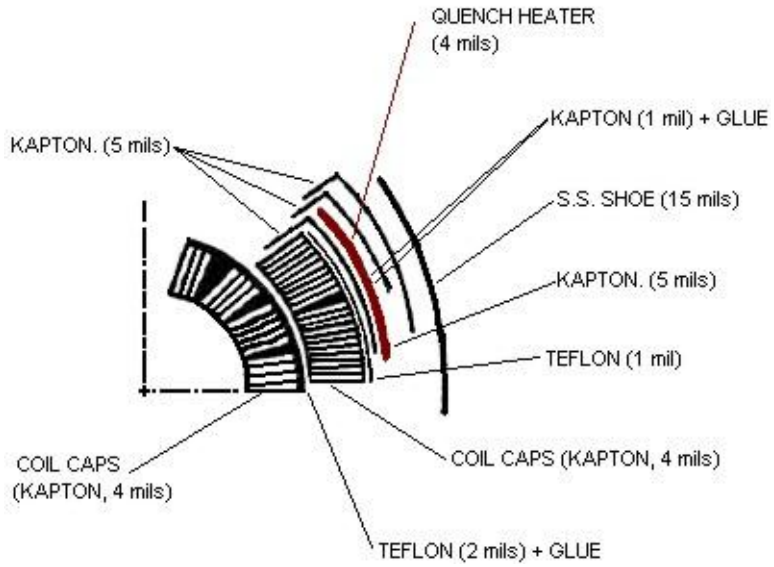

Figure 3.8 Heater Location in the LHC, Source [Ferracin & Prestemon 2009]

The insulation foil acts as a support and insulates the strips against the coils and the collar structure that is at ground potential. Each heater strip is 15 *m* long and covers the entire length of outer coil. There are two strips per coil quadrant. [Ferracin & Prestemon 2009, Rodriguez-Mateos et al. 2000, Rodriguez-Mateos 2001, Rossi 2009]

3.4.3. By-pass Diode

By-pass diodes are used for the MB and MQ type magnets. MQ magnets are the quadrupole magnets. The idea how a by-pass diode works is shown in Figure 3.9.

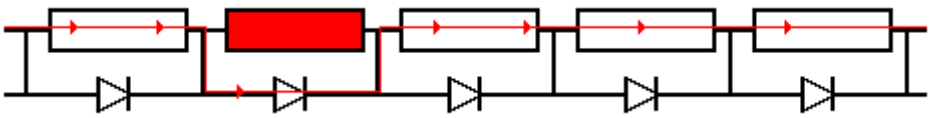

Figure 3.9 By-pass Diode During Quench

Magnets are de-coupled from the rest of the circuit using a cold by-pass diode. If a resistive voltage is detected across the magnet, it provokes a fast commutation of the current from a quenching magnet to its parallel diode. In the figure the quenching magnet is indicated with red color. [Ferracin & Prestemon 2009, Rodriguez-Mateos 2001]

3.4.4. Fast Abort of Power Supply

One means of quench protection is a fast abort of the power supply after the quench detection. The layout of this kind of protection is shown in Figure 3.10.

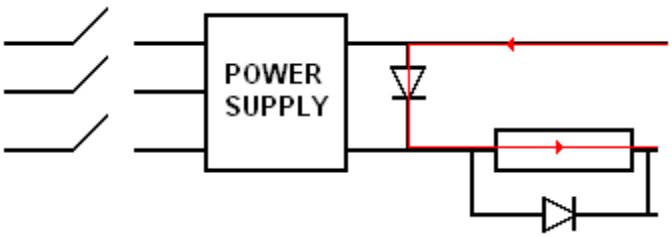

Figure 3.10 Power Supply During Quench

Sector power supply switches off the main circuit breaker after detection and as a consequence voltage falls down to zero volts. Current is still assured with a diode. [Ferracin & Prestemon 2009, Rodriguez-Mateos 2001]

3.4.5. Dump Resistors

Dump resistor protection is used in the LHC for the MB and MQ type magnets. Layout and operation of this kind of circuit is shown in Figure 3.11.

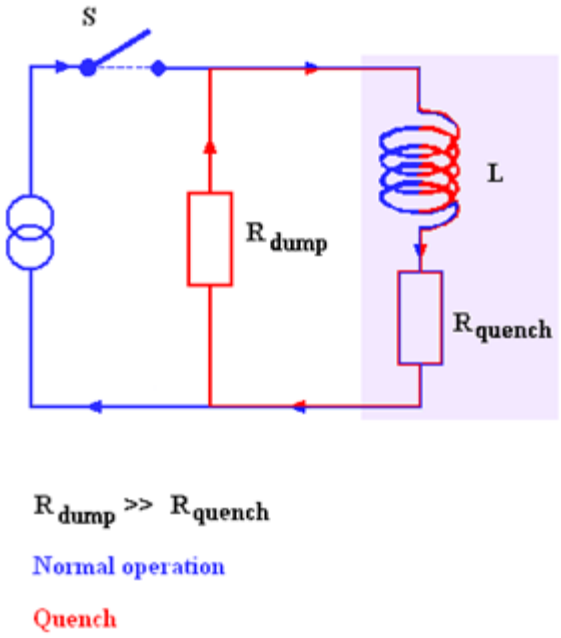

Figure 3.11 Dump Resistor During Quench

After the quench is detected, the magnet chain is de-excited by opening switches across a dump resistor. It dissipates the energy stored in the other non-quenching superconducting magnets. In the case of dump resistors not being in the circuit, energy would be dissipated very slowly over around 20 minutes in the freewheeling diode and by-pass diode. Because of the large values of inductance in the circuit, de-excitation happens slowly. Time constant is about 100 seconds for dipole circuits and about 50 seconds for quadrupole circuits. [Ferracin & Prestemon 2009, Rodriguez-Mateos 2001, SM18]

3.5. Parameters

3.5.1. MIITs

Power dissipates in a quenching magnet by the joule effect and heats up the conductor. To avoid temperature rise the heat source must be eliminated. This can be done by the means of ramping down the magnet current. As mentioned before, the maximum temperature builds up in the point where quench first started. This hot spot temperature should be kept between the limits of 77 and 127 *ºC* (350-400 *K*) for the LHC dipoles, but whenever possible, the limit should be set to -173 *ºC* (100 *K)*. Commonly, designers tend to go above this limit in order to save coil volume, conductor and hence costs. In order to design the magnet to meet these needs, one can estimate the peak temperature by the given formula:

$$Tmax = \int_0^{\infty} I^2(t)\,dt = A^2 \int_{T_0}^{T_{max}} \frac{C_p(T)}{\rho(T)} dt = U(T_{max})$$

,

where I(t) is current, t is time, A is cross-sectional area of the composite conductor, T is temperature, T_0 is base temperature, $C_p(T)$ is specific heat, and $\rho(T)$ is resistivity. For simplicity, MIITs value is often determined by multiplying the value of $U(T_{max})$ by 10^{-6}. From the equation it can be seen that by lowering the value of MIITs, one also decreases the value of the hot spot temperature. MIITs can be reduced by lowering the value of current immediately after quenching, that is to say, with the help of quench protection. As MIITs value is dependent on the protection used, one can reduce the hot spot temperature by the means of protections discussed in section 3.4. [Bhunia 2003, CAS 1996, Ferracin & Prestemon 2009, Rodriguez-Mateos 2001]

3.5.2. Quench Time Intervals

Quench heater delay time is the time interval between firing the heaters and the time when the quench is spread to all the coils and is observed. This time is generally between 30 and 60 *ms*. Quench heater delay time measures how well the quench heaters perform.

The quench validation time t_{det} is defined as the time between the detection of the quench and generation of the quench trigger firing the heaters. Detection happens when resistive voltage exceeds a predefined threshold for a given time interval. Validation time is introduced to recognize voltage spikes or noise and not detect them as real quenches. Figure 3.12 shows how the quench validation time is determined from U_QS0.

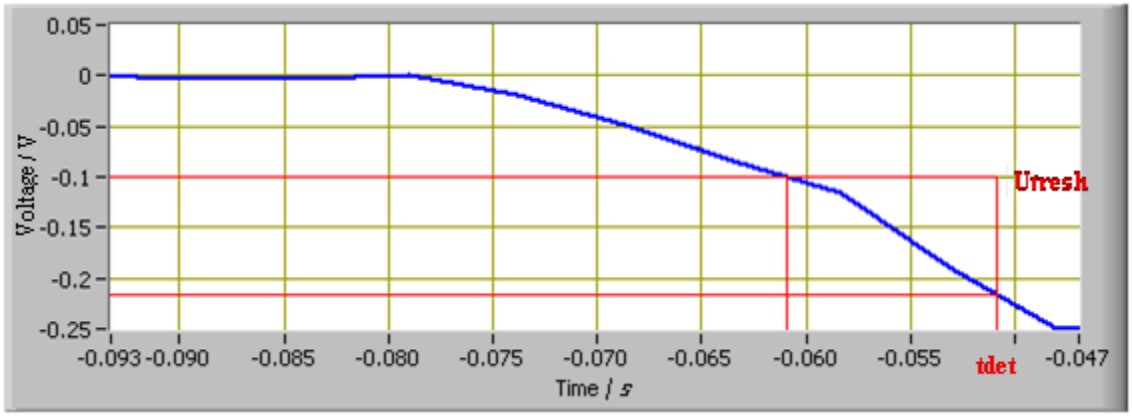

Figure 3.12 Quench Validation Time tdet from U_QS0

This example is showing a case similar to LHC detection, where voltage threshold value is set to ±100 *mV* and quench is detected when the voltage stays under this value for at least 10 *ms*. After this, changes in the voltage may happen to any direction since the triggers fire the heaters to speed up the quench propagation velocity. [Motiwala & Sridhar, Quench-analysis]

3.6. Post Mortem Analysis Software

A software tool called Post Mortem (PM) Analysis was built at CERN for hardware commissioning and Post Mortem event analyzing for the LHC. This software helps experts and accelerator operators to access and analyze the data which is generated during Electrical Circuit Commissioning or in the case of a failure during the operation of the LHC. Post Mortem tool enables browsing for different Post Mortem events, data analyzing and result management. Main reasons and events when it is used are: immediate diagnostics after beam loss, off-line analysis of post mortem event, dipole quench and support analysis for decision making. Post Mortem Analysis should give answers to questions such as, what actually happened, what was the initial point of the event, and what kind of sequence leads up to this incident. [PostM]

In the case of a failure during the LHC operation, Post Mortem information is collected from the various sub-systems. Data is analyzed within few minutes to find the cause of the failure, thanks to which, it can be quickly determined if the system can be restarted. Various machine systems are monitored to understand any malfunctions. In this way, the software helps to improve the operational efficiency and enables shorter breaks between the operations.

Figure 3.13 shows the basic idea behind Post Mortem Analysis. The idea of the post mortem is that it collects and stores data from client systems.

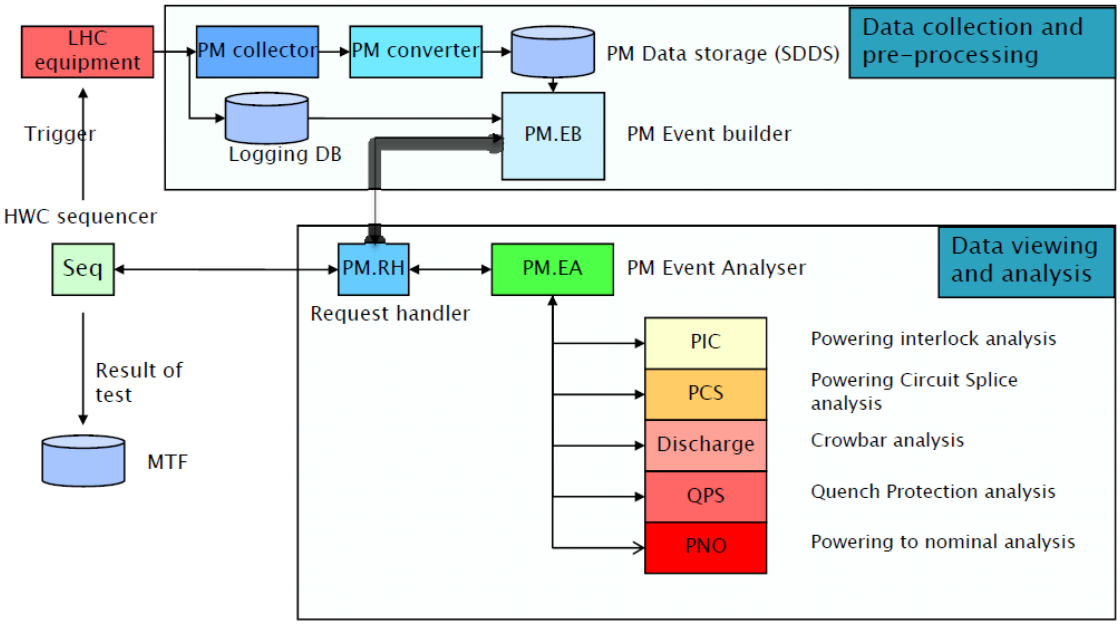

Figure 3.13 Post Mortem Analysis, Source [Andreassen 2009]

After this, it converts the data from the binary client format into a standard format (SDDS Self Describing Data Set). Because the amount of this data is huge and it needs to be analyzed quickly, it also requires huge amount of data handling. This all is done for reliable and safe operation of the LHC. [Rijllart et al. 2007]

4. METHODS

4.1. Introduction

The goal of the work leading to this thesis, was to design a quench analysis application to help experts by analyzing the quench parameters automatically from the data collected by the Post Mortem tool after a quench occurs. However, this application could also be used to analyze heater behavior, even in the absence of quench. The designed application is based on an existing application called Automatic Quench Analysis, abbreviated AQA which was used during the testing of dipole magnets in the SM18 test facility. This previous application is written with LabVIEW's graphical G-programming language and this was to be used for the designed application also. LabVIEW stands for Laboratory Virtual Instrument Engineering Workbench. With the help of AQA it is possible to do the analysis for example for training quenches of dipoles. Such parameters as quench detection times, quench location, MIITs at the time of quench, MIITs at the instant of heater discharge and MIITs at 20 *ms* after heater discharge were determined by the previous application. The application also gives alerts for various alarming conditions in the quench performance. Figure 4.1 gives brief overview between previous and new analysis tools. Post Mortem has several different analysis tools.

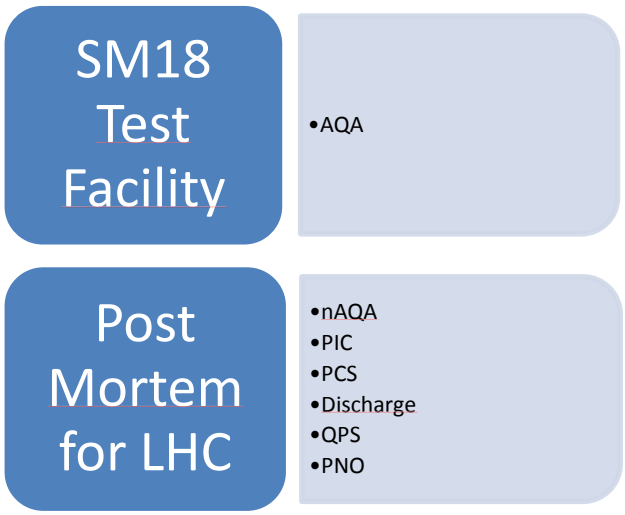

Figure 4.1 From SM18 Test Facility to Post Mortem for the Use of the LHC

Data used for the new Automatic Quench Analysis (for simplicity this is called nAQA although it serves the same basic analysis as AQA) is collected from Post Mortem system after quench protection system has reacted. Main parts of the analysis

were to be kept but due to data and measurement system changes, new design had to be carried out. With the help of designed nAQA, it is possible to save time for more important activities and reduce the time needed after quench occurrence for data analyzing and thus time needed for inactive mode of the LHC. One important task the nAQA does, is creating alarms if certain values are exceeded. Users can also modify preset alert levels. A hierarchy diagram for the designed application is shown in Figure 4.2.

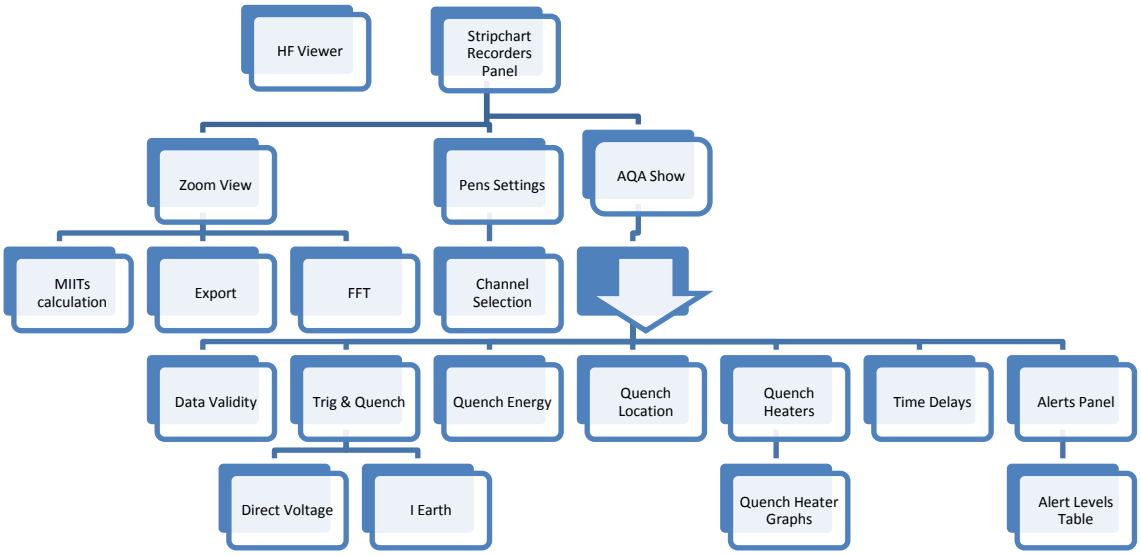

Figure 4.2 Hierarchy of Automatic Quench Analysis

The main user panels are presented at the top of the hierarchy diagram and from them, users can move into different analysis steps through different panels.

4.2. Requirements

New application was to be designed to be part of the Post Mortem system and similar reasons were behind it as with the Post Mortem. Quench protection system for the LHC had been recently renewed and requirements were set for the extension of the application to the new Quench Protection System (QPS) data as follows. As the LHC quench protection system was extended with symmetric quench detection and a bus splice monitor, data from these extensions would be integrated into the present analysis scheme and analyzed according to predefined criteria. A further development was to define a scheme to analyze multiple quenches, such as quench propagation and implement it in the defined scheme.

First of all, most of the functions of the previous application were to be kept to confirm that coil quenched safely. With the application it would be possible to see

quench signals, protection system behavior, quench detection performance and different numerical analysis values.

Since AQA was designed to be used during magnet testing in SM18 magnet test facility, modifications to the application code had to be done. SM18 test facility is used for the testing and validation of dipole magnets for the LHC. Files used by post mortem are stored in a different file format (SDDS) than before and the application had to be designed to be able to handle this format. Many of the previously monitored signals were missing from the new data and application had to be adapted to use the signals existing in SDDS-files.

During the programming, it was possible to use known quench data collected from the LHC by the post mortem system beforehand and compare the results given by the designed application and the post mortem browser to validate the results. In addition, some manually analyzed quench data from these quench events was available and because of this different values could be validated quite easily.

A decision of using LabVIEW was clear since it was possible to reuse the code from the previous AQA application. LabVIEW programming interface and language was already familiar and provided easy methods for creating applications for measurements purposes. Furthermore, LabVIEW support was available in the same section.

4.3. Design Procedure

Like with every design procedure, one was to start with research into the subject. In this case, it meant studying superconductivity, quench event, quench protection, accelerators especially in the case of the LHC and existing applications designed by the section (Post Mortem Analysis). After this, study on the existing AQA application and its parameters was done. Although LabVIEW programming language should be quite adaptable for various programmers, it was not always clear or logical what had been done before, due to the use of inherited code. A quite easy method with graphical programming would be to follow the rule “from left to right” but since this had not been always followed it was difficult to see which parts happened before the others. Code had also almost no commenting and some functions were hiding under each other which made understanding the application behavior sometimes difficult. This might be due to version change, which also hid some of the numbers in the code or made them show up incorrectly. Some problems with the configuration files were found when they did not show up correctly after modification due to previous file versions from word or excel which were not recognized anymore by LabVIEW. Some problems were also faced with the computer settings. Settings for decimals had to be in “.”-form instead of “,” to make sure LabVIEW understands decimal readings.

Since original application was designed with older version of LabVIEW, project was commenced by converting all the non-compatible functions in the subVIs to be compatible with the LabVIEW version 8.6. SubVIs are LabVIEW subprograms which

imitate virtual instruments. After this, the data reading from SDDS-buffers was implemented to the code. The previous application was understanding time of quench as the x-axel point zero. Zero point from the SDDS-data was chosen to be when I_REF signal reaches 0 amperes, and because of this, all the data read from the buffers was changed to understand this point as the reference point. After this, data could be fed to all the subVIs, which were to do the analyses. By comparing the values shown or missing in the panels, decisions could be made of the further development of the application and its subVIs.

Sometimes some previously existing measurement signals were missing in the data collected from the LHC and different approaches were chosen to be able to do the analysis. Electrical circuits in the tunnel conditions differed from the SM18 circuits and this created some difficulties in evaluating the correspondence between some of the signals. Signals were either named differently or they might have had the same name but were measuring different things and this created confusion. This was the case, for example, with MIITs calculation because current measurement signal I_MEAS was not the same one which was expected by the previous application. In the previous application I_MEAS was measuring current across a magnet, whereas now in the tunnel across the whole circuit. Amplitudes between different measurement signals from SDDS had to be adjusted to correspond those ones expected by the application, and it was not always clear which amplitude had been used before.

The previous application was dividing different measurement signals for different circular buffers depending on their frequency. This approach was not followed in the designed application, instead three different circular buffers were used. Dump resistance signals U_DUMP_RES and T_RES_BODY got their own buffers which saved the data in X, Y form since they did not have constant frequency. Other signals were saved in the buffer in X, dX, Y form, the same way the previous application was handleing all the signals. Later on, the measurement signals are called by their name for the use of the analysis.

The previous code was designed to read some of the information directly depending on the file names, and the application was sometimes expecting them to be in a certain kind of form. This time, the file names were composed differently and all the information could not be read directly from the file names. For example, the date information still existed on the SDDS file names but the identification method had to be changed for the designed application. In the SDDS file system, the date format also varied between different folders. The measurement signal configuration was also changed compared to the previous application and a new configuration file was created where all the information was used by the application later on. According to the configuration file, the user can, for example, choose which signals to show in the six graphs of the front panel. Information of the SDDS channel order and signals used in the analysis are shown in Table 4.1. A code was added for checking if the read signals correspond to the signals and signal positions in the file configuration. If this is not the case, signal positions are set to the positions in the file configuration, and missing or

additional signals are indicated for the user. After the configuration and file reading were done, the analysis functions could be applied and these are discussed in the following chapter.

Non-compatibility between Windows and Linux also created problems in the design phase since many of the users did not use Windows and application had to be converted also for Linux. Especially, in between different releases of the application, converting to Linux was not very efficient. In addition, LabVIEW was not very competent in enabling many coders to be working with the same code at the same time although newer versions of LabVIEW enable code sharing.

Table 4.1 Measurement Signals for New Application

Signal Name	**Signal Description**
RT_REF	50 *Hz*
I_ERR_MA	Current Loop Error (*mA*) 50 *Hz*
I_DIFF_MA	Measurement difference (*mA*) 50 *Hz*
I_EARTH_PCNT	Earth Fault Current (*kA*) 50 *Hz*
I_REF	Current Reference (*kA*) at 50 *Hz*
I_MEAS	Current Measurement (*kA*) at 50 *Hz*
V_REF	Voltage Reference at 50 *Hz*
V_MEAS	Voltage Measurement at 50 *Hz*
I_DIFF	Created from I_DIFF_MA by Converting to *kA*, 50 *Hz*
I_ERR	Created from I_ERR_MA by Converting to *kA*, 50 *Hz*
I_REF	Current Reference at 100 *Hz* (*kA*)
I_MEAS	Current Measurement at 100 *Hz* (*kA*)
V_REF	Voltage Reference at 100 *Hz*
V_MEAS	Voltage Measurement at 100 *Hz*
I_MEAS	Measured Current (*kA*) at 1 *Hz*
V_MEAS	Measured Voltage at 1*Hz*
U_LEAD_POS	Voltage Across Current Lead 1 *Hz*
U_LEAD_NEG	Voltage Across Current Lead 1 *Hz*
R_LEAD_POS	Calculated from U_LEAD_POS/I_MEAS 1 *Hz*
R_LEAD_NEG	Calculated from U_LEAD_NEG/I_MEAS 1 *Hz*
I_EARTH	Earth Current (*kA*)
U_2	Voltage Across Internal Aperture
U_1	Voltage Across External Aperture
U_QS0	Voltage difference between U2-U1
U_HDS_1	Quench Heater Voltage 1
U_HDS_2	Quench Heater Voltage 2
U_HDS_3	Quench Heater Voltage 3
U_HDS_4	Quench Heater Voltage 4
T_RES_BODY_1	Temperature 1 of Dump Resistance
T_RES_BODY_2	Temperature 2 of Dump Resistance
T_RES_BODY_3	Temperature 3 of Dump Resistance
U_DUMP_RES	Voltage of Dump Resistance

Since the previous application was with the older version of LabVIEW there were some changes which had to be done for compatibility reasons. Non-compatible subVIs and equation functions were changed to subVIs, which were supported by the novel version, and data accuracy was changed to be more precise. The old accuracy gave huge differences to the results shown, but after changing to double precision this problem was eliminated. The version change also produced some differences on the front panel object locations.

A good amount of time was used for the user interfaces since they were lacking user-friendly designs, for example, with the colors and the lining of the objects. Many of the graphs were missing important units, signal names or explanations, which were added. SubVIs which the user could use to do the signal selection were changed to use tables in showing signal names and their descriptions instead of single text line which did not manage to line the objects properly. Figure 4.3 shows one of the user panels for nAQA.

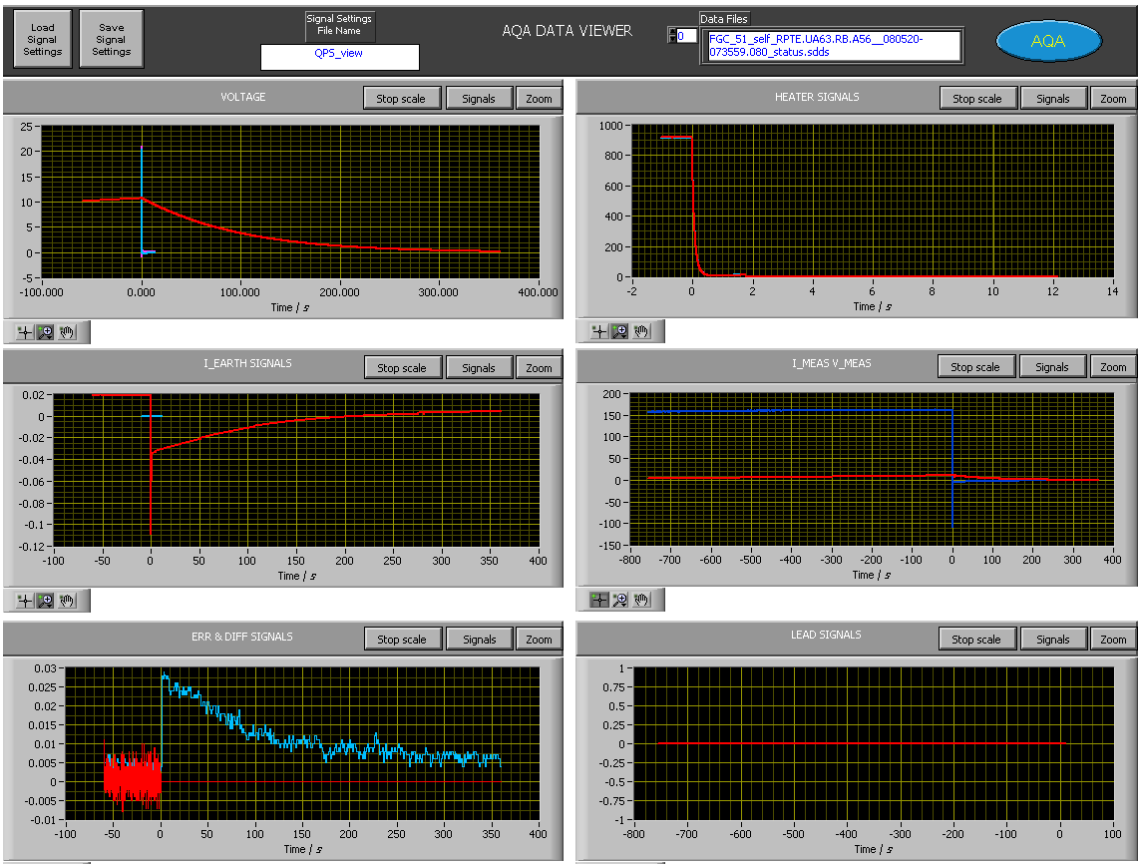

Figure 4.3 Data Viewer Panel

The application loads automatically predefined signal settings to be shown on the graphs and gives user the possibility of changing the view of these signals (colors, line styles, line widths etc.). In addition to the Data Viewer panel, the application automatically opens the Automatic Quench Analysis panel from where user can navigate to see more specific results from different analysis steps.

4.4. Analysis Steps

The most important parts of the quench application are the different analysis steps. The analysis steps are divided in the application to seven different steps which include: data validity, trigger and quench, quench energy, quench location, quench heaters, time delays and alerts panels (Figure 4.4).

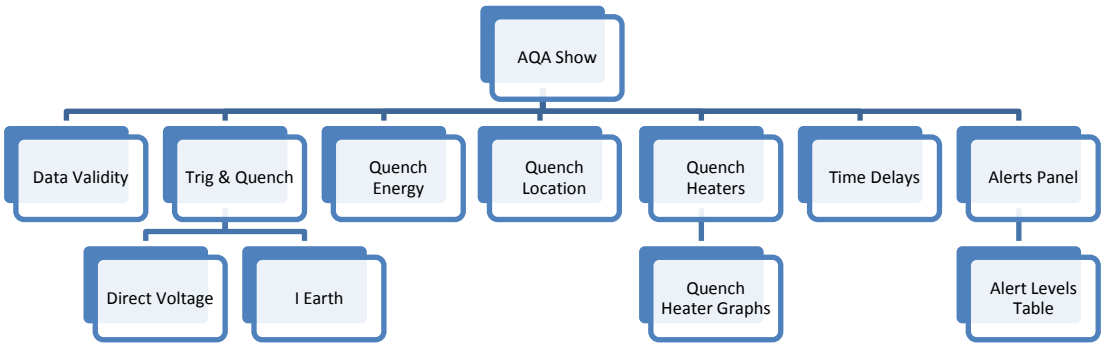

Figure 4.4 Hierarchy of Quench Analysis

For all these analysis steps either minor or major changes were made. All of them were changed to read signals according to the SDDS signal names and to alert users if some of the signals are missing. A code was added to recognize if some of the analysis steps signals do not exist. In this case, the application does not try to do the analysis in vain, which might eventually stop the application in one of the VIs. In this way some of the analysis steps could be done even if files or signals for other analyses are missing. The AQA panel shows the most important parameters collected from these analyses and highlights all the warnings and alerts from them (Figure 4.5).

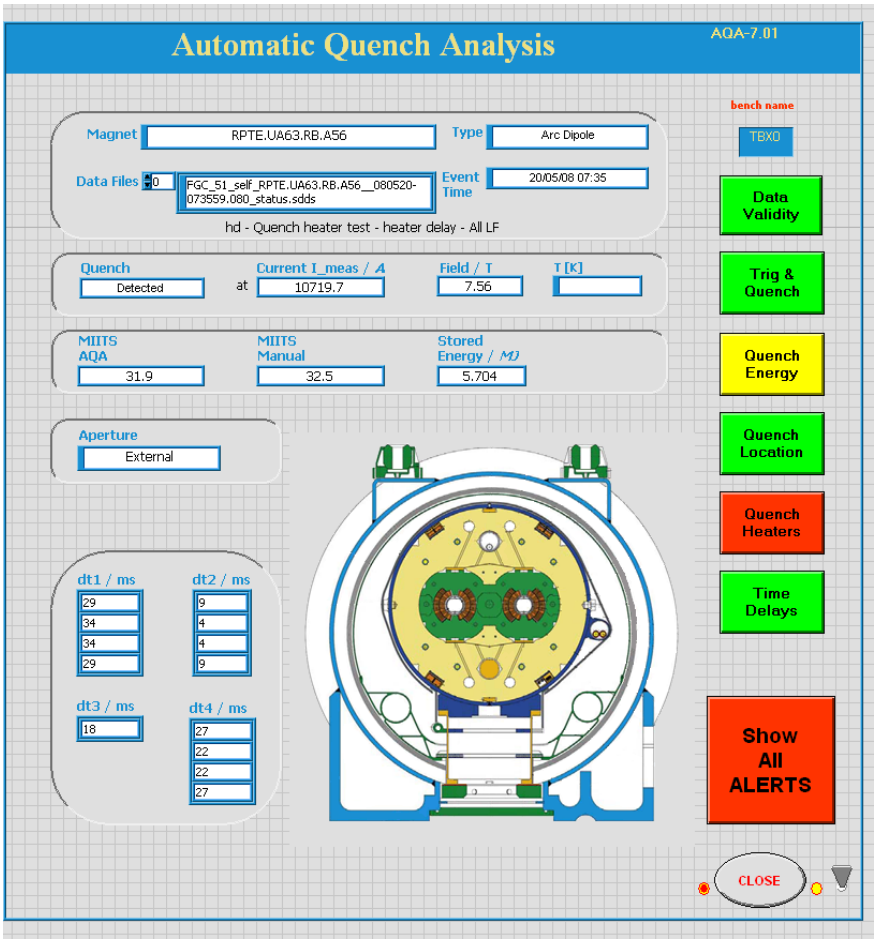

Figure 4.5 Panel for Automatic Quench Analysis

For the *data validation*, the program code was modified to check for the existence of different FGC-files under the given path which are needed for the analysis steps. Post mortem stores files to different folders depending on what functions of the circuit those signals are monitoring. FGC refers to Function Generator/Controller. The signals have been stored under FGC to different buffers (iloop, ileads, status and iearth) and data validation is checking that these files are not missing. If some of them are missing, a warning is displayed to the user. A code was added to check that all the configuration files are found where they are expected to be. If not, naturally a warning is shown.

The quench detection for *trigger and quench* was reformed to use the voltage values of U_1 and U_2 and to check the voltage difference U_QS0 between these signals. If this value reaches 100 *mV* for at least 10 *ms*, a detection of the quench is made. Also, a check for U_1 and U_2 reaching "first value ±200 *mV*" was added to recognize possible symmetric quenches which would remain unnoticed in the U_QS0 signal. If U_1 or U_2 reaches a threshold of 200 *mV* before U_QS0 reaching 100 *mV*, a warning is shown to the user. In addition, the aperture where the quench started is determined with U_QS0 from the sign of the signal, when it reaches the limit value of ±100 *mV*. Since U_QS0=U_2-U_1 it gives a negative value if U_2 is the first one to change value (external location). If U_1 is the first to change value it gives a positive

value (internal location). After this, the real beginning of the quench is calculated with a derivate from U_QS0 before the quench detection time. This is because the quench actually starts a while before it is detected. Actual quench time Tq is determined by derivating U_QS0, U_1 or U_2 values from two seconds before the detection time until the detection time Td. This curve is checked for a change in the derivate values and cutting slope into two slopes at this point as seen in Figure 4.6. After that, change rate of the second slope is studied. If it is fast, the first slope is fitted with one curve and checked if this fitted curve meets Y=0 *V*. If not, start of the second slope is taken as actual quench time. If 0 voltage reaching time is found in the fitted curve, this point is taken as the actual quench time.

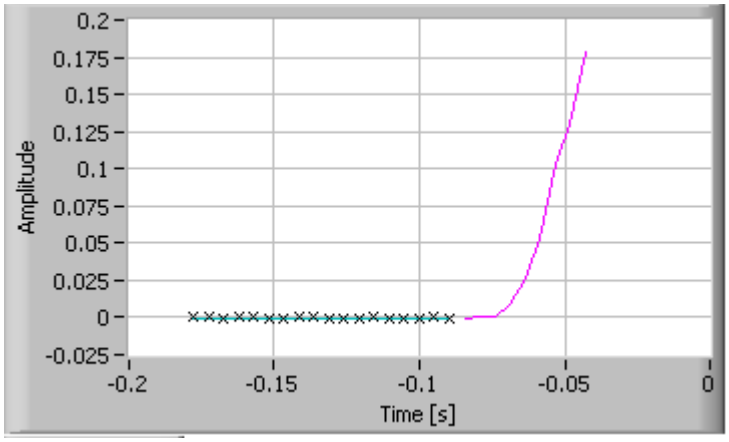

Figure 4.6 Fast U_QS0 Slope Cut to Two Curves to Find Tq

In the case of a slow second slope as seen in Figure 4.7, first part of the curve is cut to two additional parts which are both fitted with curves to find 0 voltage reaching time. Actual quench time Tq is then taken from the first curve to reach zero. Depending on the number of fitted lines used for the Tq analysis, shape of the signal is indicated to user either as L (single line), L+L (double line) or L+L+L (triple line in the case of slow changing slope).

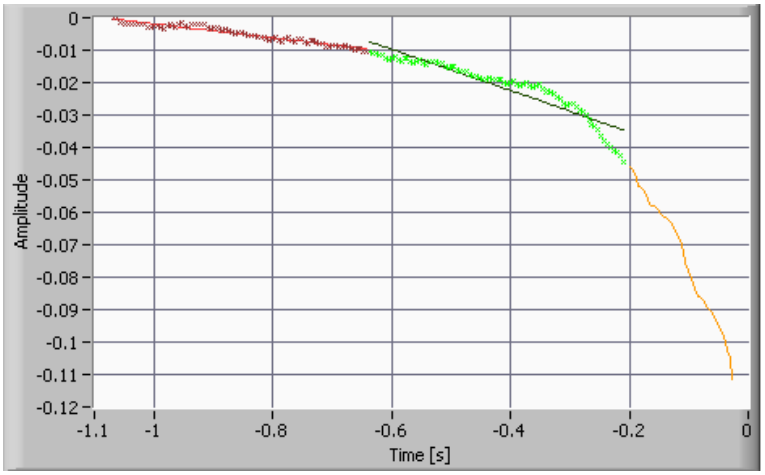

Figure 4.7 Slow Changing U_QS0 Slope Cut to Three Curves to Find Tq

Some of the other values in the trigger and quench analyses could not be determined, since signals for these were not available anymore.

For the *quench energy* analysis an approach to find MIITs values had to be determined again. First of all, MIITs calculations for the hall probe values were removed because all of the hall probe signals were missing. This is due to the fact that during SM18 testing, more monitoring of the signals and analyzing was needed than at present in the tunnel conditions. Also the MIITs value after 20 *ms* of heater discharge could not be trusted anymore and it had to be removed. SM18 test conditions differed from the LHC tunnel conditions mainly so that there was no diode and they have different heater power supplies. In the case of MIITs calculations, measurement signal I_MEAS in the tunnel is the current in the whole circuit, not just over the quenching magnet as previously. The renewed MIITs calculation is based on an interpolation model. It is calculating MIITs based on dipole magnets nominal current of 11.85 *kA*. The interpolation values for the dipole magnets are given in Table 4.2 and they can be considered to give high enough accuracy for the MIITs calculation model.

Table 4.2 MIITs Interpolation Values for Dipoles

MB		**Current / *A***	**MIITs after validation / MA^2s**
10	1	11850	33.31
9	0.9	10665	31.83
8	0.8	9480	30.18
7	0.7	8295	28.41
6	0.6	7110	26.44
5	0.5	5925	24.22
4	0.4	4740	21.53
3	0.3	3555	18.10
2	0.2	2370	13.57
1	0.1	1185	7.54

A graph for the given interpolation values is shown in Figure 4.8 where the MIITs values have been plotted against the current. The values have certain trend which they are following and behavior can be predicted from the graph.

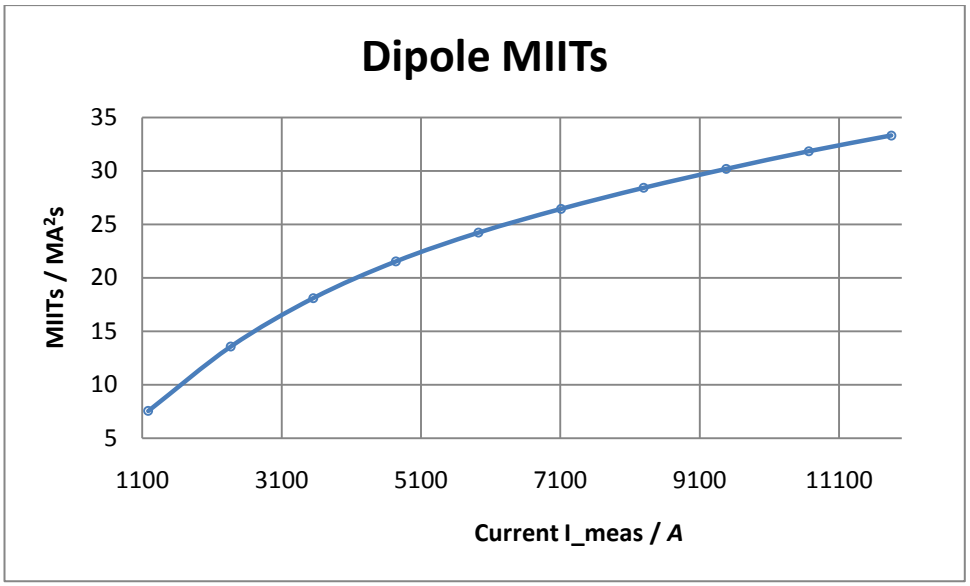

Figure 4.8 MIITs Model Graph for Dipole Magnets

Same kind of interpolation was made for the quadrupole magnets (Table 4.3).

Table 4.3 MIITs Interpolation Values for Quadrupoles

MQ		**Current / *A***	**MIITs after validation / *MA²s***
10	1	11850	26.55
9	0.9	10665	25.24
8	0.8	9480	23.85
7	0.7	8295	22.38
6	0.6	7110	20.82
5	0.5	5925	19.21
4	0.4	4740	17.83
3	0.3	3555	17.84
2	0.2	2370	17.37
1	0.1	1185	14.79

Figure 4.9 shows how the MIITs model behaves differently for the quadrupole magnets. In comparison to dipole graph, quadrupole curve is not as predictable. Between 3600 and 4800 amperes, curve has a kind of a plateau. Under these values, the MIITs value falls sharply.

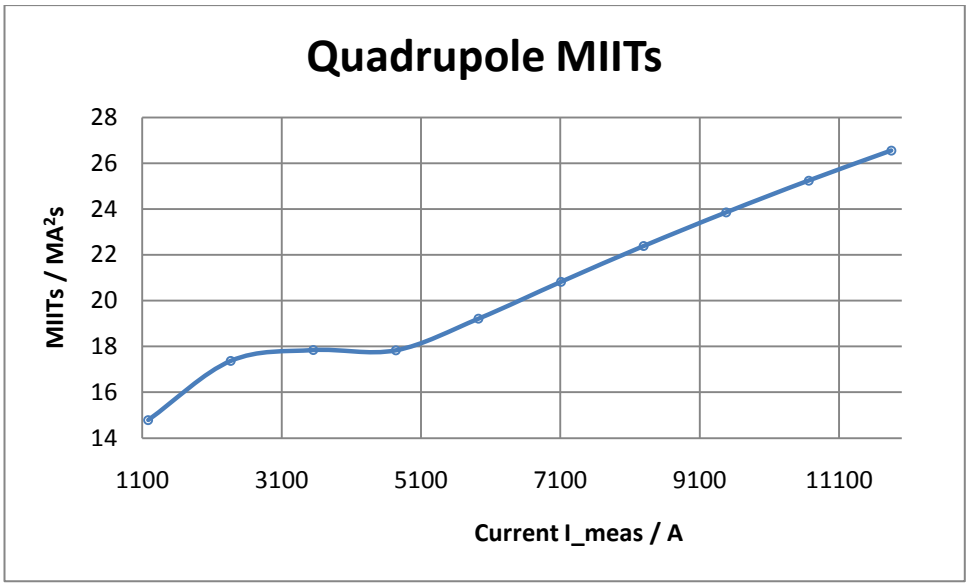

Figure 4.9 MIITs Model Graph for Quadrupole Magnets

The *quench location* gives the user information in which aperture the quench started and this is already determined in the trigger and quench analysis. The previous application gave information on the pole, the layer and the section of the quench location. With the LHC tunnel data, the user is simply informed if the quench started in the external or the internal aperture. In the case of symmetric quench when aperture voltages U_1 and U_2 are detected to reach simultaneously limit value of 200 *mV*, application gives information of "external / internal" location. In the case that no quench is detected from U_QS0 or location could not be determined for some other reason, application gives the information "Not determined" as location. A figure of a dipole showing the location of the quench and heater information has also been added as an additional button.

The quench heater data was completely missing the quench current signals in tunnel conditions. Quench heater voltage signals U_HDS1-4 were used for the heater voltage analysis and the current was calculated based on the U_HDS values and a constant resistant value which was known to be 11.3 Ω. Furthermore, current values were set to have a value differing from zero when the voltage value is dropping. All the values before and after the voltage drop were set to zero (==0.1 *A*). An example for the current values in comparison to the voltages is shown in Figure 4.10.

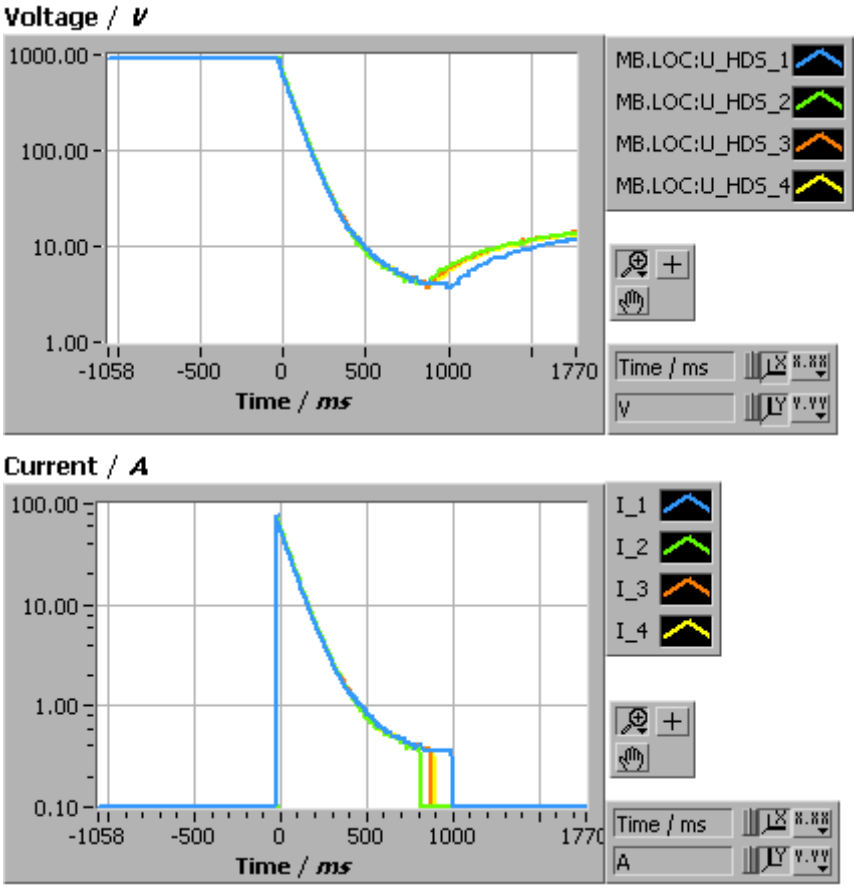

Figure 4.10 Quench Heater Voltage and Current

A completely novel analysis step for the *time delays* and the differences between triggers was added. The analysis gives information if, for example, the detection or the triggering did not happen in time. For the analysis, quench detection time tD from U_QS0=100 *mV*, heater firing time tFire from U_HDS, trigger time tTrigger from I_REF=0 *A* and time tDump from U_DUMP_RES=100 *V* were determined. They should appear in the order of tD < tFire < tDump < tTrigger. The application gives an alarm if this is not the case. Alarms are given if tD, tFire or tDump are bigger than 0 *s*, since tTrigger should be the last signal to appear and it should virtually be zero due to the nature of the application. The time difference calculations between following trigger times are calculated given that all the signals exist in following fashion: dt1=tFire-Td, dt2=tDump-tFire, dt3=tTrigger-tDump and dt4=tTrigger-tFire. The application gives warnings or alarms, if differences could not be calculated, or if time differences turn out to be too big.

Alert level values were checked to match desired limits for the new circuits and all these values were collected in a file. The previous application was reading many of the alert level values from the program code, and this was changed so that the users would have easy access if they want to modify the alert levels. A table showing all the alert levels was added to the code so that limit values could be checked during the operation easily.

The previous program code had all the signal names spread through all the VIs and this was changed so that when any of the signals were needed it was read from a file or a global. This was done to ensure that signal names could be easily changed for analyses with different magnets such as quadrupoles which have different signal configurations. The same approach was used for file paths and some parameters like threshold values and resistance values which might not always be the same.

5. RESULTS

5.1. Quench Data

To validate the values given by the application, data consisting of current values between 757 … 11123 *A* was used. Mostly twelve different quench events are used in this report, but data was always studied with at least 36 different quench events to validate the results. Most of these events have current value above 10000 *A* but there also exists some quench data from lower currents of 2000 *A* which is due to the quench at injection phase. For normal quenches where change in U_QS0 is detected before change in U_1 or U_2, following quench events are used:

- training quench from 06.05.08 18:12:16 with current of 10651 *A,*
- training quench from 07.05.08 17:53:50 with current of 10714 *A,*
- training quench from 16.05.08 17:22:26 with current of 10834 *A,*
- training quench from 20.05.08 07:35:59 with current of 10720 *A,*
- training quench from 21.05.08 18:17:47 with current of 10944 *A,*
- training quench from 26.05.08 07:41:44 with current of 10996 *A* and
- training quench from 04.06.08 08:55:16 with current of 11123 *A.*

Symmetric quench data is also used to make sure all the alarms are working properly in the case of unexpected situations. Following quench events are used for this purpose:

- training quench from 23.05.08 07:44:16 with current of 10976 *A,*
- quench from 17.03.10 02:23:15 with current of 2035 *A* and
- transmission-line effects quench from 30.03.10 08:51:17 with current of 2271 *A.*

So called quenchino events, where quench seems to occur but voltages do not stay above threshold long enough, were also studied. For this purpose, events from following dates were used:

- beam induced quench from 18.04.10 22:33:40 with current of 757 *A,* quenching magnet being B20R1 and
- beam induced quench from 18.04.10 22:33:40 with current of 757 *A,* quenching magnet being A20R1.

In addition, data with some unexpected missing signals is used to make sure, that application does not stop working if signals are missing and gives all expected alarms. The application is also tested with normal signals without any quench to make sure no quench is detected and that all the signals are shown as expected. For the non-existing quench, data from 10.04.08 at 21:30:22 is used. From different data analysis steps, especially quench detection times, quench energies, initial locations, heater voltages, time delays and differences are studied.

5.2. Results for Quench Detection

A very important parameter of quench protection is the detection of quench at a correct time. Results from the application are studied by visually looking at the changes from the graphs and then comparing these to the results detected with the application. For all the graphs shown in this chapter U_1 is pink, U_2 is light blue and U_QS0 is dark blue. The tables show results for threshold reaching times Td. Threshold value for detecting a quench for U_QS0 is ±100 *mV* and for U_1 and U_2 change of 200 *mV* compared to the first value. Actual quench time Tq is also shown for all the events and it has been calculated from the first signal reaching threshold.

First, results from normal quenches, when change in U_QS0 is detected before change in U_1 or U_2, are studied. After that, symmetric quench detection is studied. Zero point at X-axel is set to be the event time taken from I_REF signal dropping to zero amperes. Bear in mind that U_QS0 is the difference between changes in U_1 and U_2 and it has been magnified to show the changes in order to detect the quench earlier. In ideal situation, threshold reach in U_QS0 is detected before threshold reach in U_1 and U_2.

First, quench data graph from 06.05.08 at 18:12:16 is shown in Figure 5.1. Change in U_QS0 becomes visible after -0.0741 *s* already when the curve starts to rise. U_2 curve begins to lower about 10 *ms* later at -0.064 *s*.

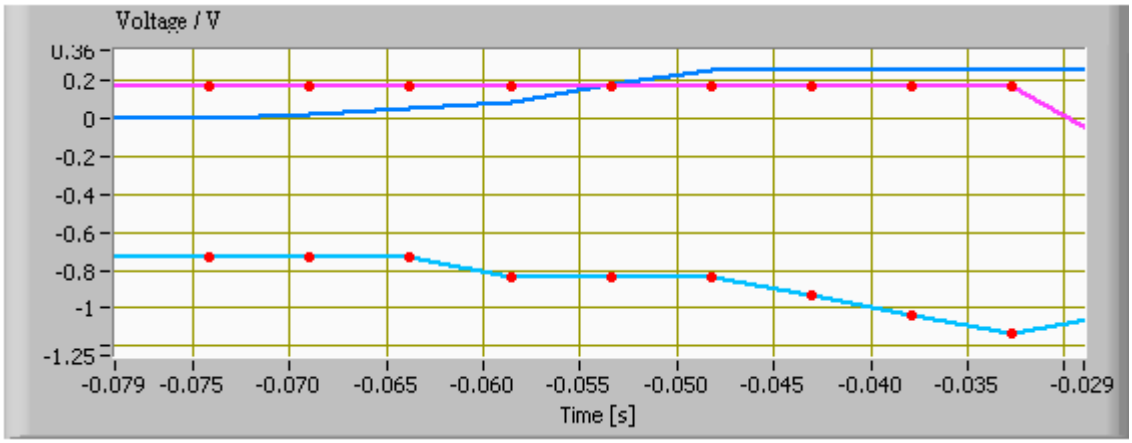

Figure 5.1 Quench from 06.05.08 at 18:12:16. U_1 is pink, U_2 is light blue and U_QS0 is dark blue.

The detected values for threshold reaches with the new application are shown in Table 5.1. First signal to reach the threshold is U_QS0 followed short after by U_2 and U_1.

Table 5.1 Detected Values for 06.05.08 at 18:12:16

Signal Name	Td / s
U_QS0	-0.058583
U_2	-0.043115
U_1	-0.029257
Tq	-0.0741

Quench data from 07.05.08 at 17:53:50 is shown in Figure 5.2. Decrease in U_QS0 is happening already at -0.073 *s* which is before noticeable change in U_1 and U_2. First rise in U_1 begins at -0.047 *s*.

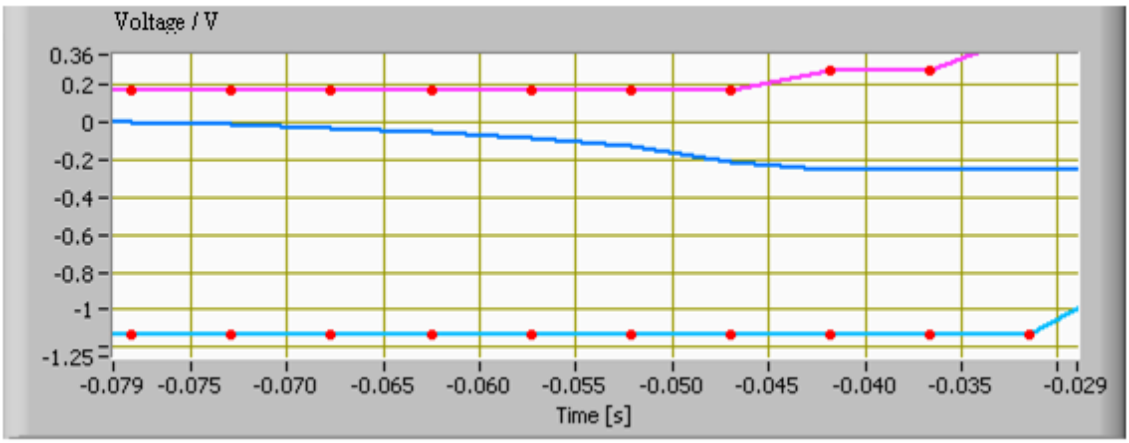

Figure 5.2 Quench from 07.05.08 at 17:53:5., U_1 is pink, U_2 is light blue and U_QS0 is dark blue.

The detected values for same event are shown in Table 5.2. Again, U_QS0 is detected to reach the threshold first being followed by U_1 and U_2.

Table 5.2 Detected Values for 07.05.08 at 17:53:50

Signal Name	Td / *s*
U_QS0	-0.057329
U_1	-0.041859
U_2	-0.028001
Tq	-0.0729

Quench data from 20.05.08 at 07:35:59 is shown in Figure 5.3. U_QS0 curve declines starting at -0.079 *s* and U_1 rises rapidly at point -0.053 *s*.

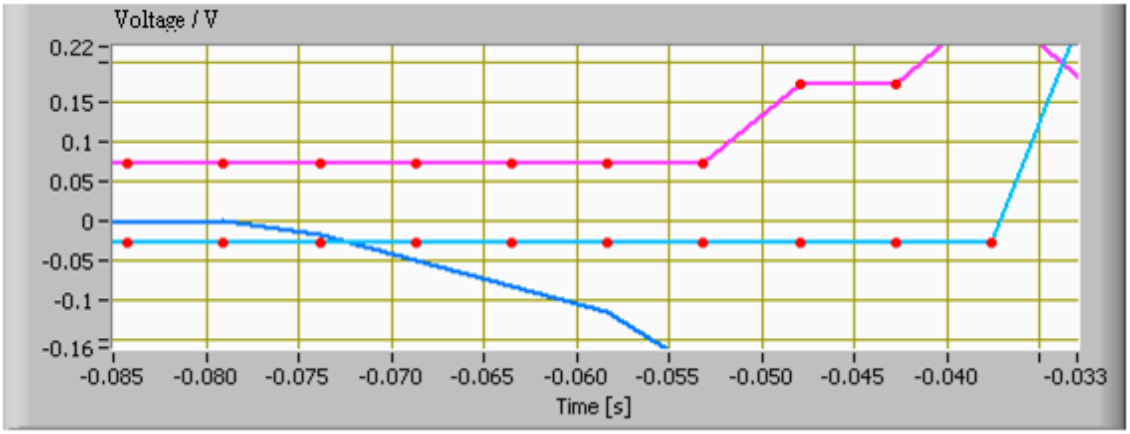

Figure 5.3 Quench from 20.05.08 at 07:35:59. U_1 is pink, U_2 is light blue and U_QS0 is dark blue.

The values detected by the application are shown in Table 5.3. Threshold reach in U_QS0 is detected as expected before threshold time in U_1 and U_2.

Table 5.3 Detected Values for 20.05.08 at 07:35:59

Signal Name	**Td / *s***
U_QS0	-0.058328
U_1	-0.037679
U_2	-0.034180
Tq	-0.0790

Quench data from 16.05.08 at 17:22:26 is shown in Figure 5.4. A visible ascend in U_QS0 begins at -0.0813 *s* and first visible change downward in U_2 begins at -0.071 *s*.

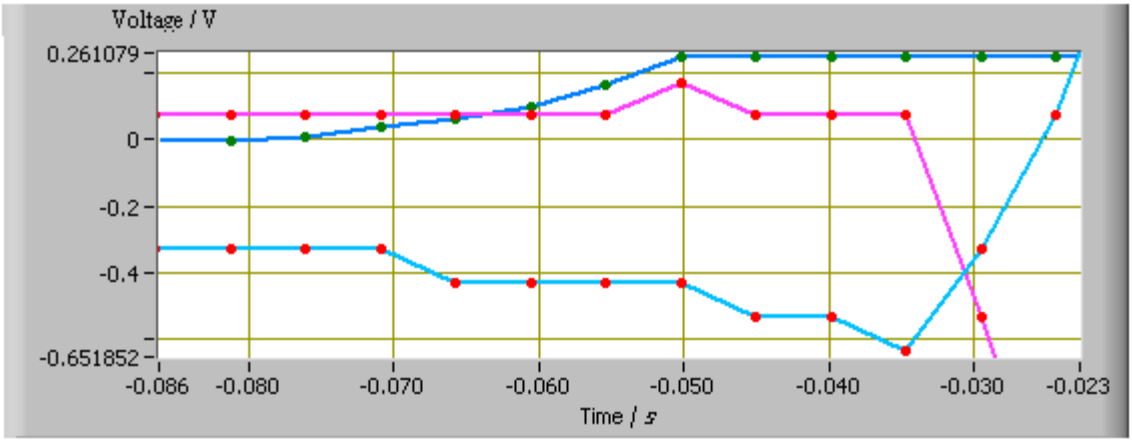

Figure 5.4 Quench from 16.05.08 at 17:22:26, 10834., U_1 is pink, U_2 is light blue and U_QS0 is dark blue.

The detected values for the new application are shown in Table 5.4. Voltage signal U_QS0 reaches threshold before U_1 and U_2.

Table 5.4 Detected Values for 16.05.08 at 17:22:26

Signal Name	**Td / *s***
U_QS0	-0.060584
U_2	-0.045115
U_1	-0.033836
Tq	-0.0761

Quench data from 21.05.08 at 18:17:47 is shown in Figure 5.5. Curve of U_QS0 begins upward change after -0.0801 *s* and first visible descend in U_2 begins at -0.064 *s*.

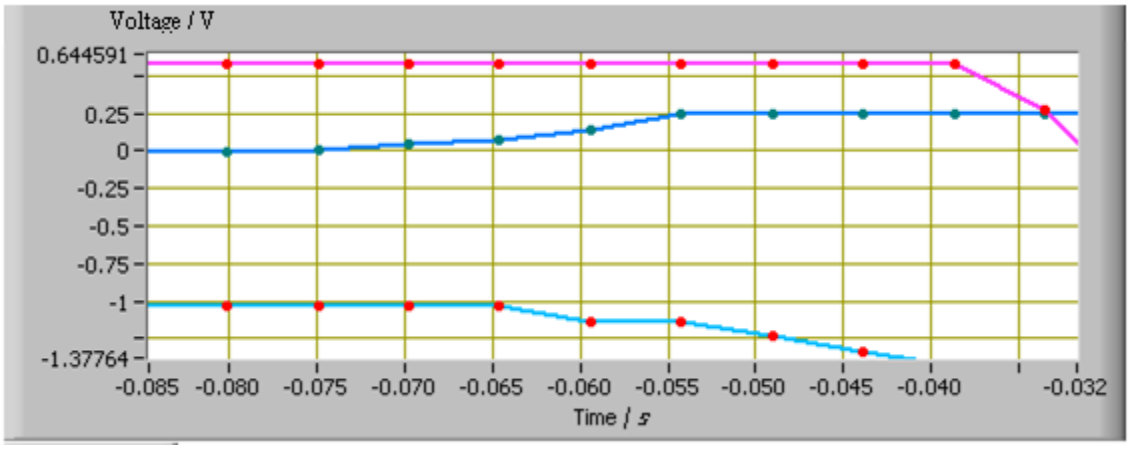

Figure 5.5 Quench from 21.05.08 at 18:17:47. U_1 is pink, U_2 is light blue and U_QS0 is dark blue.

The detected values for the new application are shown in Table 5.5. Change in U_QS0 is detected again before change in U_1 and U_2 which is expected.

Table 5.5 Detected Values for 21.05.08 at 18:17:47

Signal Name	**Td / *s***
U_QS0	-0.064584
U_2	-0.049115
U_1	-0.035258
Tq	-0.0749

Quench data from 26.05.08 at 07:41:44 is shown in Figure 5.6. Voltage in U_QS0 is visibly increasing around -0.0661 *s*. First visible decline in U_2 is seen at -0.04 *s*.

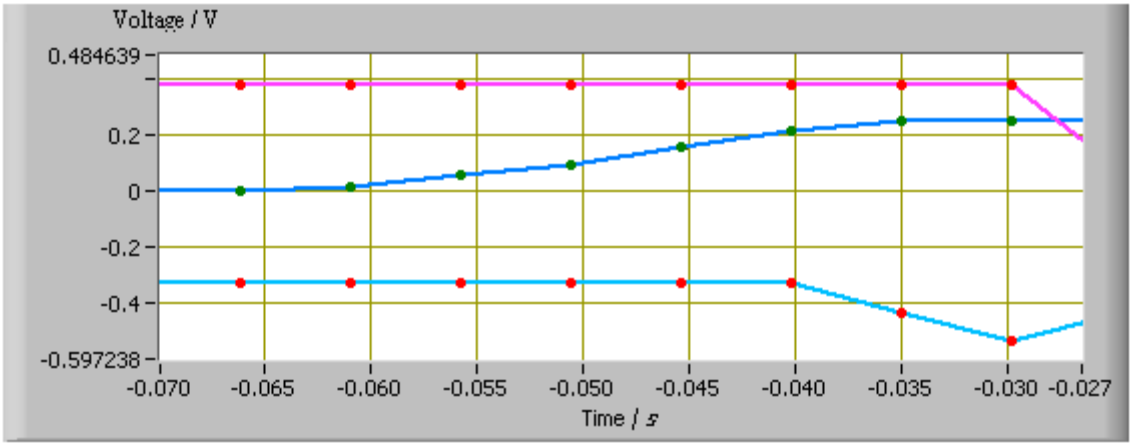

Figure 5.6 Quench from 26.05.08 at 07:41:44. U_1 is pink, U_2 is light blue and U_QS0 is dark blue.

The detected values for the new application are shown in Table 5.6.

Table 5.6 Detected Values for 26.05.08 at 07:41:44

Signal Name	**Td / *s***
U_QS0	-0.050586
U_2	-0.029929
U_1	-0.026428
Tq	-0.0661

Quench data from 04.06.08 at 08:55:16 is shown in Figure 5.7. Decrease in U_QS0 starts visibly around -0.075 *s* and first visible increase in U_1 is at -0.59 *s*.

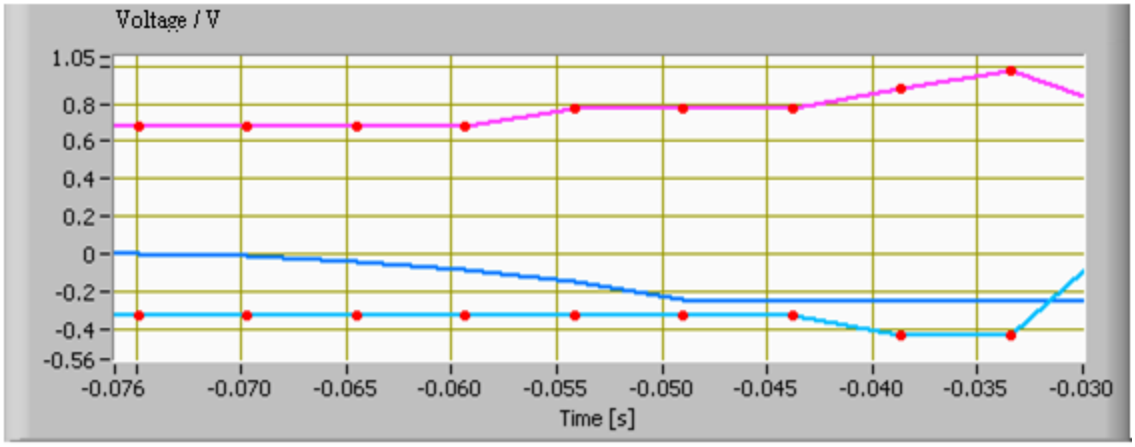

Figure 5.7 Quench from 04.06.08 at 08:55:16. U_1 is pink, U_2 is light blue and U_QS0 is dark blue.

The detected values for the new application are shown in Table 5.7.

Table 5.7 Detected Values for 04.06.08 at 08:55:16

Signal Name	**Td / *s***
U_QS0	-0.059329
U_1	-0.038679
U_2	-0.030337
Tq	-0.0749

Next, symmetrical quenches where U_1 and U_2 change so symmetrically that their difference might not be detected with U_QS0, are studied. For this reason, U_1 and U_2 values reaching 200 *mV* are detected often before U_QS0 reaching 100 *mV*. First quench data from 23.05.08 at 07:44:16 is shown in Figure 5.8. Clearly seen from U_1 and U_2, at the time of -0.035 *s* something is happening in the circuit. U_QS0 does not detect this change though and only begins to slowly decline at -0.03 *s*.

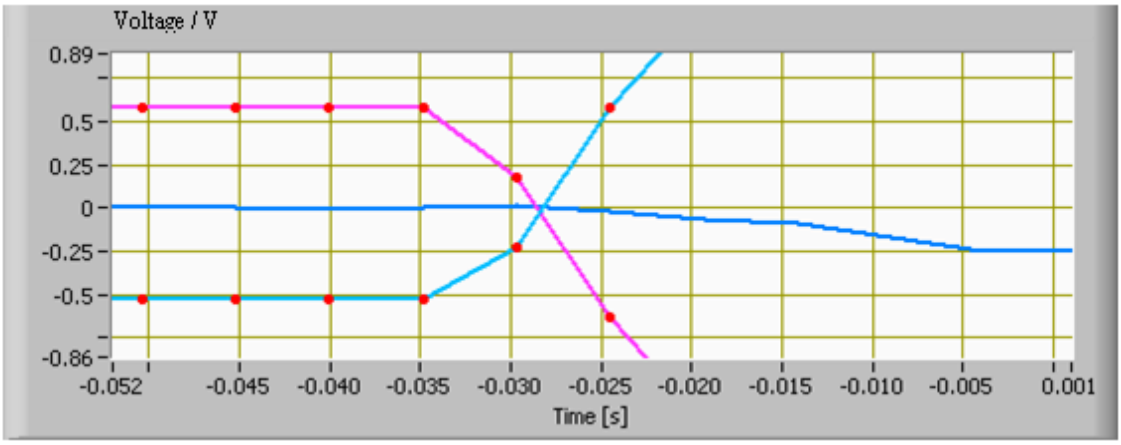

Figure 5.8 Symmetric Quench from 23.05.08 at 07:44:16. U_1 is pink, U_2 is light blue and U_QS0 is dark blue.

The detected time values for the new application are shown in Table 5.8. Although very symmetrical, times for U_1 and U_2 differ from each other and they both reach their threshold before U_QS0.

Table 5.8 Detected values for 23.05.08 at 07:44:16

Signal Name	**Td / *s***
U_1	-0.032284
U_2	-0.031426
U_QS0	-0.014131
Tq	-0.0349

Next, symmetrical quench data from 17.03.10 at 02:23:15 is shown in Figure 5.9. Visible change in all of the signals seems to happen at -0.0134 *s*.

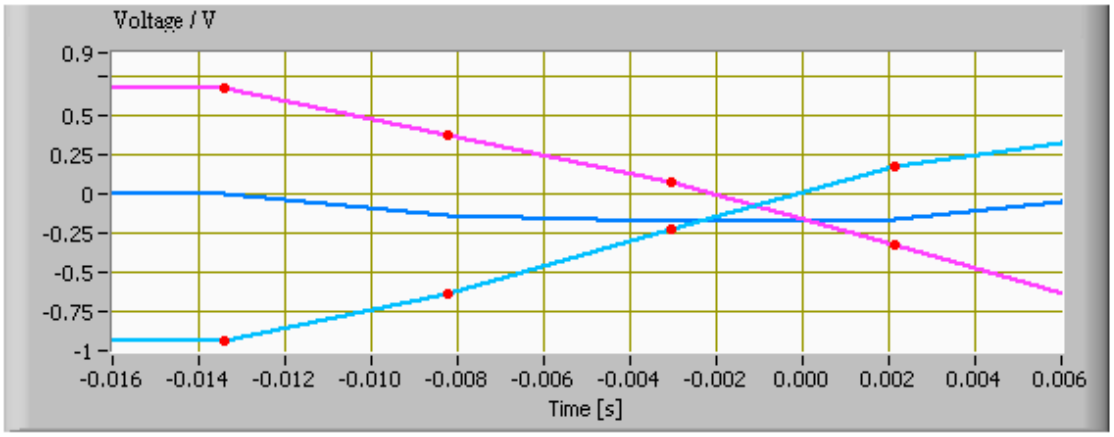

Figure 5.9 Symmetric Quench from 17.03.10 at 02:23:15. U_1 is pink, U_2 is light blue and U_QS0 is dark blue.

The detected values for the new application are shown in Table 5.9. U_1 and U_2 both reach their threshold before U_QS0.

Table 5.9 Detected Values for 17.03.10 at 02:23:15

Signal Name	**Td / *s***
U_1	-0.009971
U_2	-0.009971
U_QS0	-0.008222
Tq	-0.0134

Symmetric quench data from 30.03.10 at 08:51:17 is shown in Figure 5.10. As can be seen U_1 and U_2 change symmetrically beginning at -0.0267 s. In this case U_QS0 is detecting the change at the same moment also and starts to decrease. This quench was due to transmission line effects.

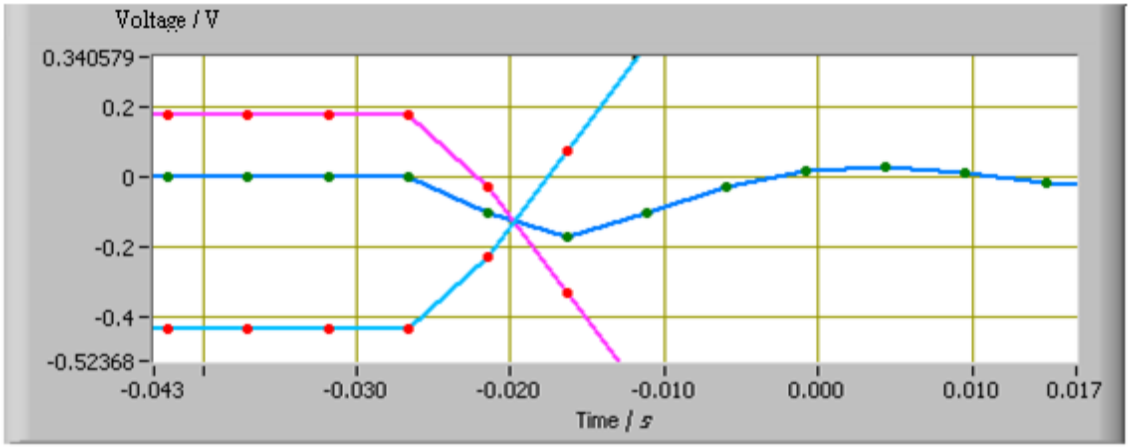

Figure 5.10 Symmetric Quench from 30.03.10 at 08:51:17. U_1 is pink, U_2 is light blue and U_QS0 is dark blue.

Detected values in Table 5.10 show that threshold is reached first in U_1 and U_2 although there is not much difference in time.

Table 5.10 Detected Values for 30.03.10 at 08:51:17

Signal Name	**Td / *s***
U_2	-0.021540
U_1	-0.021540
U_QS0	-0.021505
Tq	-0.0267

Quenchino data from 18.04.10 at 22:33:40 for magnet A20R1 as shown in Figure 5.11 shows another kind of situation. U_QS0 detects a change at -0.052 *s* but stays under -100 *mV* just little above 10 *ms* which is just enough to be detected as a quenchino. First visible decrease in U_2 is seen at -0.036 *s*.

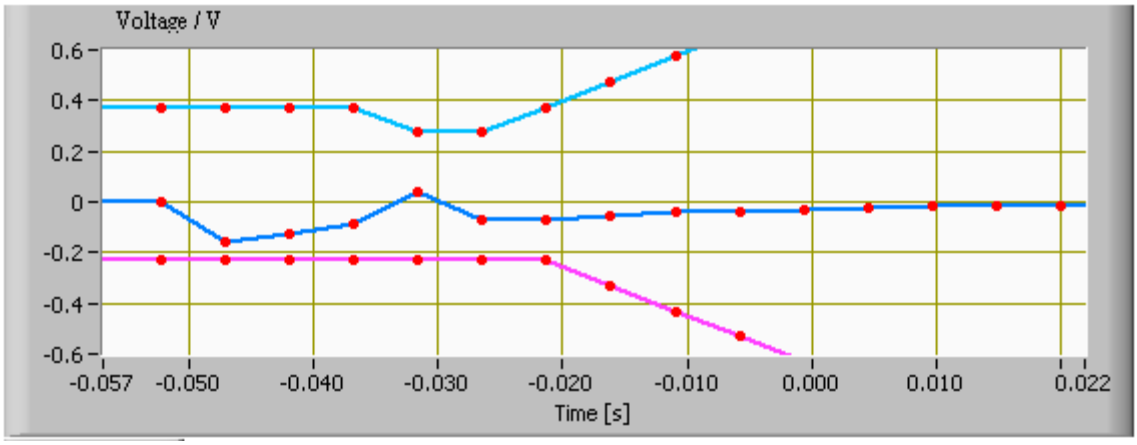

Figure 5.11 Symmetric Quench from 18.04.10 at 22:33:40 from A Magnet. U_1 is pink, U_2 is light blue and U_QS0 is dark blue.

Detected values in Table 5.11 show that U_1 and U_2 reached the threshold simultaneously. However, U_QS0 reached threshold before them and in this case application also detected it even if U_QS0 did not stay long under the threshold limit.

Table 5.11 Detected Values for 18.04.10 at 22:33:40

Signal Name	**Td / *s***
U_QS0	-0.047213
U_1	-0.011027
U_2	-0.011027
Tq	-0.0524

Similar kind of quenchino data from 18.04.10 at 22:33:40 is shown in Figure 5.12. This is the same event time as for previous quenchino data but for different magnet in the circuit. Magnet is B20R1. Voltage U_QS0 starts to decline at -0.052 *s*. This is before U_1 and U_2 which are changing noticeably and symmetrically only at -0.022 *s*.

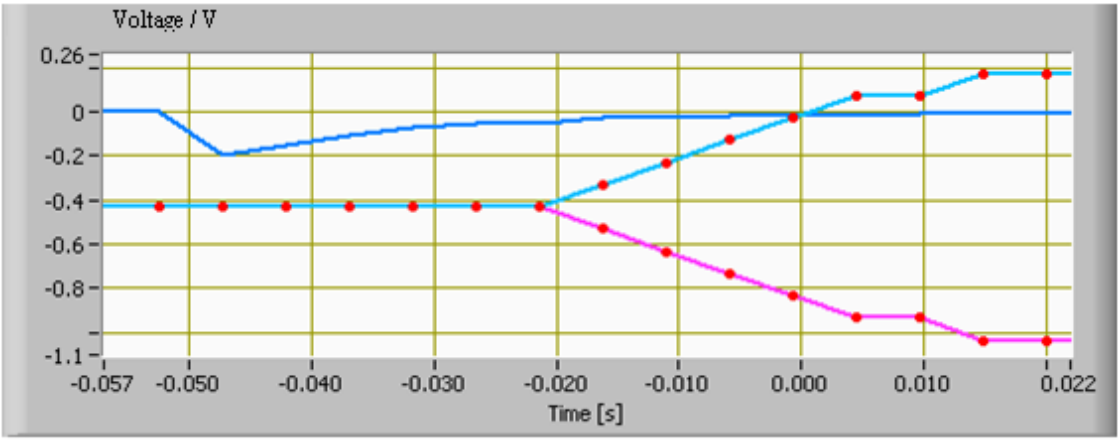

Figure 5.12 Symmetric Quench from 18.04.10 at 22:33:40 from B Magnet. U_1 is pink, U_2 is light blue and U_QS0 is dark blue.

The detected values for the new application are shown in Table 5.12. Again, U_QS0 is detected to reach the threshold before U_1 and U_2. Voltage signals U_1 and U_2 change symmetrically but quenchino is actually induced by beam.

Table 5.12 Detected Values for 18.04.10 at 22:33:40

Signal Name	**Td / *s***
U_QS0	-0.047213
U_2	-0.011027
U_1	-0.011027
Tq	-0.0524

In the case of a missing path, the application informs the user of missing signals and does not give number values for Td. The case of present signals but not showing quench is studied. To make sure no quench is detected when it is absent, data from 10.04.08 at 21:30:22 is used and graph for this data is shown in Figure 5.13.

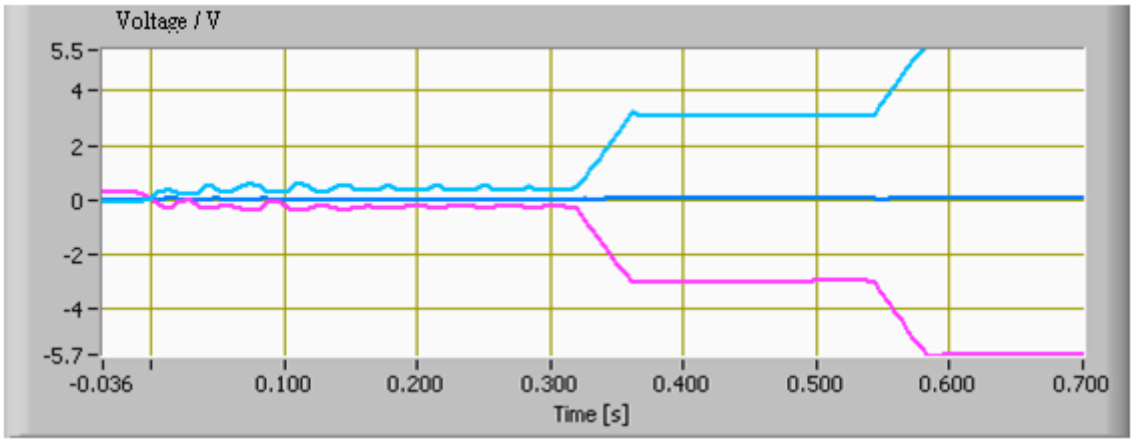

Figure 5.13 Non-quench Data from 10.04.08 at 21:30:22. U_1 is pink, U_2 is light blue and U_QS0 is dark blue.

The detected values for the same event are shown in Table 5.13.

Table 5.13 Detected Values for 10.04.08 at 21:30:22

Signal Name	**Td / *s***
U_2	-0.000463
U_1	-0.000463
U_QS0	Not a number
Tq	Not a number

As can be seen, U_QS0 never reaches the threshold and application thus does not give numerical value for Td. Voltage signals U_2 and U_1 both reach the threshold symmetrically but this is not enough to detect a quench. Actual quench time Tq is not calculated if U_QS0 is not reaching threshold.

5.3. Results for Quench Energy

Next, the results for quench energy analysis are shown. Table 5.14 shows the results from the application for maximum value for I_meas, MIITs, field and stored energy. These values are especially important because by following the MIITs value we can follow the peak temperature where the quench eventually started. The higher the MIITs value, the higher the hot spot temperature. If MIITs is too high the only way to decrease it is by the means of quench protection.

Table 5.14 Results for Quench Energy Analysis

Date	Current / *A*	MIITs / MA^2s	Field / *T*	Stored Energy / *MJ*
06.05.08 18:12:16	10651	31.8	7.508	5.633
07.05.08 17:53:50	10714	31.9	7.551	5.698
16.05.08 17:22:26	10834	32.0	7.634	5.822
20.05.08 07:35:59	10720	31.9	7.555	5.704
21.05.08 18:17:47	10944	32.2	7.710	5.938
23.05.08 07:44:16	10976	32.2	7.732	5.972
26.05.08 07:41:44	10996	32.2	7.746	5.993
04.06.08 08:55:16	11123	32.4	7.833	6.128
17.03.10 02:23:15	2035	11.9	1.439	0.208
30.03.10 08:51:17	2271	13.1	1.607	0.259
18.04.10 22:33:40	757	5.4	0.536	0.029

Figure 5.14 is showing these values on a graph.

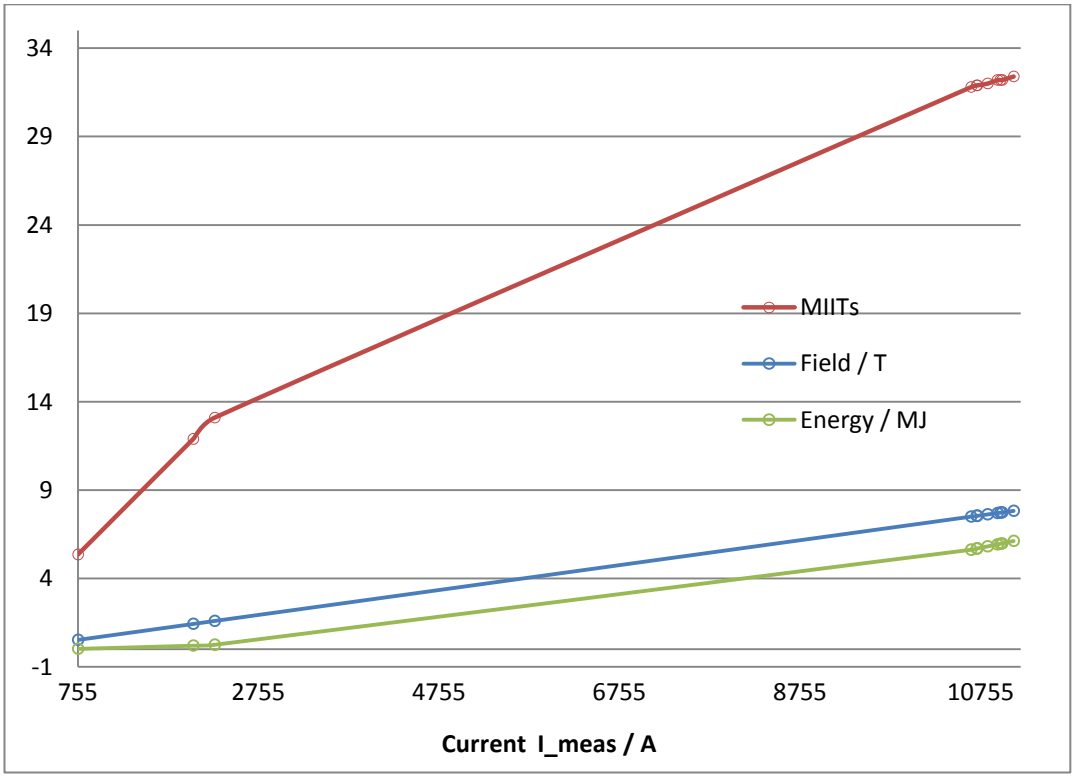

Figure 5.14 Graph for Quench Energy Analysis

Figure 5.15 shows close-up values for MIITs above 10000 *A*, since more data is available at higher currents. For the graph, more quench events were used than is shown in Table 5.14.

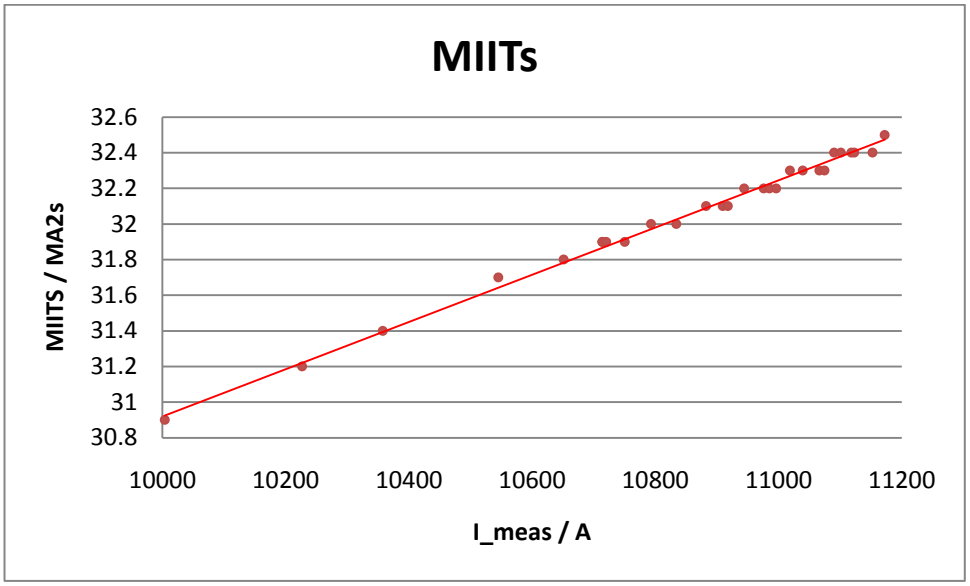

Figure 5.15 MIITs Graph for High Currents

All the tests were with the quenching magnet being a dipole, which leaves the quadrupole MIITs untested.

If a path needed is missing, the application informs of the missing signals and does not give numerical values for quench energy analysis. If data from a non-quench event is used, MIITs is still calculated according to the maximum current value. The application is giving the information that no quench is detected from the data.

5.4. Results for Quench Location

Quench location information is important because other quench parameters may vary according to the initial quench location. For example, according to the location, hot spot temperature may result in higher values, which is important to notice. In the case of tunnel conditions, only information on two locations is available. However, all the magnets have been tested before in SM18 test conditions when more information was available and differences between different specific locations have been studied.

Quench location analysis gives results for different quench events as shown in Table 5.15.

Table 5.15 Results for Quench Location Analysis

Date	Location
06.05.08 18:12:16	Internal
07.05.08 17:53:50	External
20.05.08 07:35:59	External
16.05.08 17:22:26	Internal
21.05.08 18:17:47	Internal
26.05.08 07:41:44	Internal
04.06.08 08:55:16	External
23.05.08 07:44:16	External
17.03.10 02:23:15	External
30.03.10 08:51:17	Ext / Int
18.04.10 22:33:40	External
10.04.08 21:30:22	Not determined

The different location possibilities which the new application can give are external, internal, not determined and ext / int. Location “External” is given if U_1 reaches threshold before U_2. In Figure 2.5 this would correspond to the aperture situated at the left. Location “Internal” is given if U_2 reaches threshold before U_1. Location “Not determined” is given if there is no quench detected in the given data. Location “Ext / Int” is given in the case of a symmetric quench when threshold values are reached simultaneously. All of these possibilities are present in the given data.

5.5. Results for Quench Heaters

Quench Heater analysis panel shows a graph for quench heater voltage signals U_HDS_1-U_HDS_4 and calculated values based on these signals on other graphs. Other graphs include tau, current, Tau’/Tau (%) and capacitance. These values are especially important because in the case of a quench, heaters firing properly can save the magnet from serious damage. They help the quench to propagate faster which is important since quench can damage the magnets in just few milliseconds. The faster the quench is detected and spread around the magnets, the less damage.

Four measured quench heater voltage signals are shown in Figure 5.16. In the case of this event quench heaters fired on the point of -27 and -22 milliseconds. After this, decay in the voltages can be seen. Data from 20.05.08 is used to show which kind of graphs are expected.

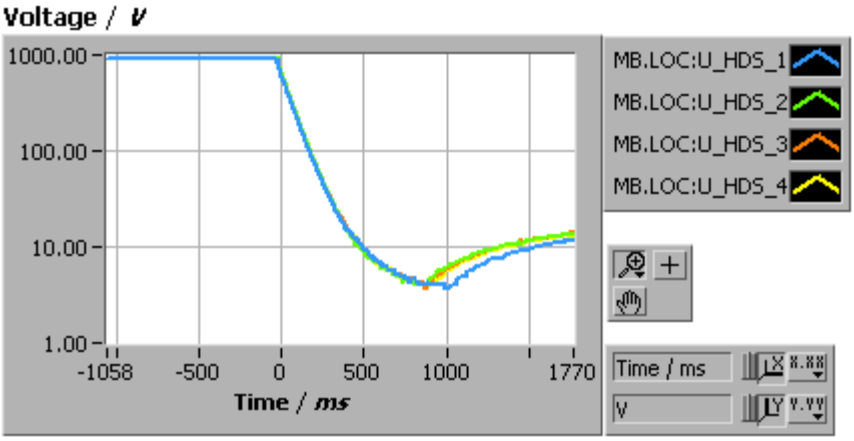

Figure 5.16 Quench Heater Voltage Graphs

Figure 5.17 shows time constant Tau graph calculated from the quench heater voltages to help the operators who are analysing quench heater behavior.

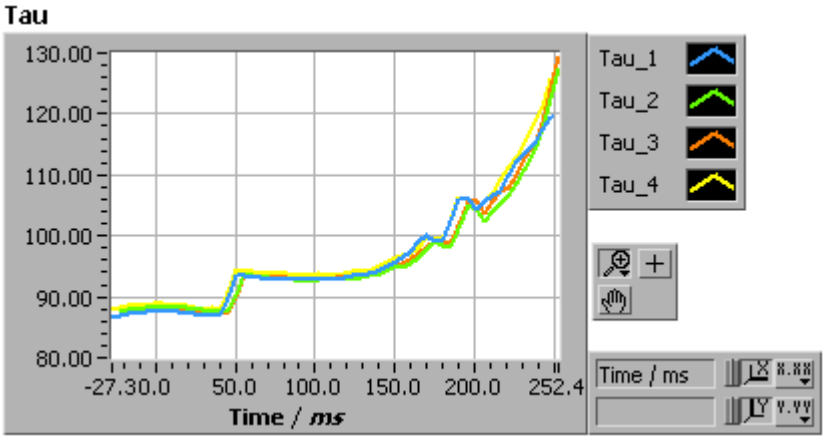

Figure 5.17 Quench Heater Tau Graphs

Figure 5.18 shows how the current graph is expected to look like. Values differ depending on the quench heater voltage values, since the resistance is constant. Values before quench heater firing and after voltage decay have been set to zero.

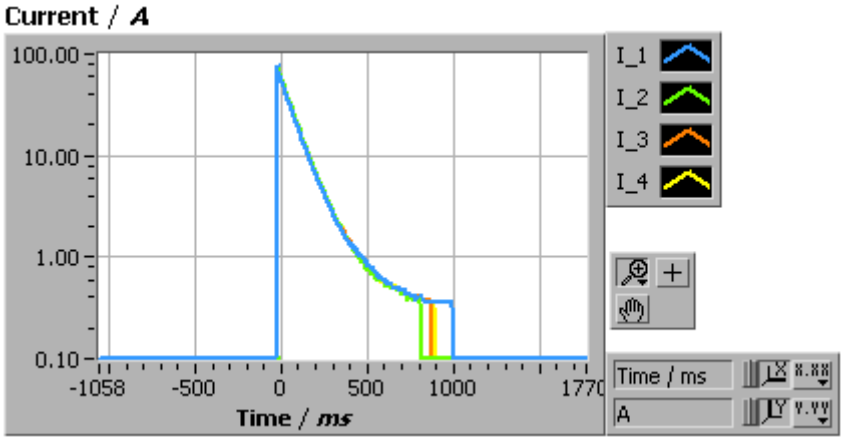

Figure 5.18 Quench Heater Current Graphs

Figure 5.19 shows Tau'/ Tau graph.

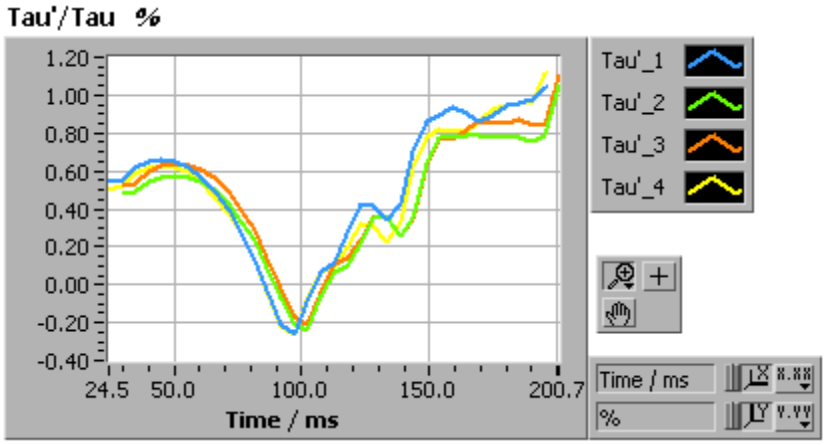

Figure 5.19 Quench Heater Tau'/ Tau Graphs

Figure 5.20 shows the capacitance graph.

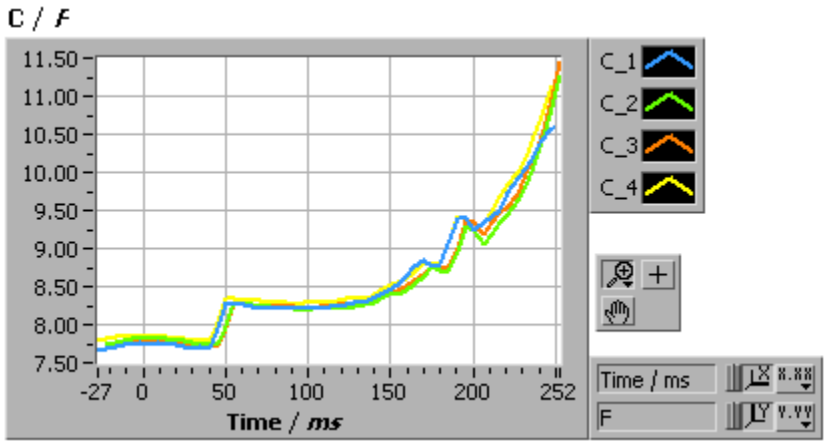

Figure 5.20 Quench Heater Capacitance Graphs

In addition, the quench heater panel shows a table for different quench heater parameters. Explanations for calculated parameters are as follows: tFire is Time of

quench heater voltage firing, Vinit_test is initial voltage, Imax is maximum current value from Vmax/Rinit, tmaxI is time of “maximum current-tFire”, Vmin is minimum voltage, tminV is time of “minimum voltage-tFire”, Tau_IniV is initial time constant, TauJmpV is highest value of Tau'/Tau and E is energy calculated from integral of $(U^2)/R$ between T(Vmax) and T(Vmin). Table 5.16 shows some typical values for quench heater voltages U_HDS_1-4 in the case of normal quenches. In addition to these ones, user is informed of values for resistances and capacitance.

Table 5.16 Results for Quench Heater Voltage Analysis for Normal Quenches

Date	**tFire / *ms***	**Vinit_test / *V***	**Imax / *A***	**Vmin / *V***	**tminV / *ms***	**TauIniV**	**TauJmpV**	**E / *J***
06.05.08	-22	904	78.0	3.1	1300	87	1.4	3135
18:12:16	-22	911	78.5	3.1	1372	88	1.5	3222
	-22	908	78.1	4.0	880	88	1.3	3183
	-22	901	77.2	4.0	1000	87	1.4	3095
07.05.08	-21	924	76.3	4.3	824	87	1.1	2999
17:53:50	-26	928	81.5	4.0	938	86	0.9	3389
	-26	927	81.5	3.4	1093	86	1.0	3387
	-26	930	81.4	3.7	1083	85	1.0	3324
20.05.08	-27	918	77.37	3.7	1020	87	1.0	3138
07:35:59	-22	917	77.7	4.0	829	88	1.1	3157
	-22	918	77.5	3.7	896	88	1.1	3134
	-27	920	77.2	3.7	917	89	1.1	3138
16.05.08	-24	909	72.6	3.7	1196	85	1.1	2698
17:22:26	-24	907	77.2	3.4	1051	84	1.2	3019
	-24	907	76.8	3.7	912	83	1.2	2971
	-30	909	76.8	3.7	1041	83	1.2	2967
21.05.08	-23	936	72.8	4.0	1114	89	2.0	2854
18:17:47	-23	927	72.0	3.4	1357	89	1.6	2797
	-28	933	82.0	3.4	1279	88	1.3	3604
	-28	935	81.7	3.4	1171	87	1.3	3504
26.05.08	-25	921	71.7	4.3	1042	91	1.5	2806
07:41:44	-30	915	75.8	3.4	1212	89	0.9	3066
	-25	918	75.8	3.4	1249	91	1.4	3137
	-30	920	75.5	3.1	1321	89	1.6	3028
04.06.08	-28	921	81.2	3.4	1145	89	0.9	3516
08:55:16	-28	923	80.8	3.7	1020	90	1.0	3512
	-28	912	79.7	4.0	886	91	0.9	3458
	-33	923	80.0	3.1	1103	90	0.8	3448

Table 5.17 shows the same values in the case of symmetric quenches.

Table 5.17 Results for Quench Heater Voltage Analysis for Symmetric Quenches

Date	tFire / *ms*	Vinit_test / *V*	Imax / *A*	Vmin / *V*	tminV / *ms*	TauIniV	TauJmpV	E / *J*
23.05.08	22	911	80.1	3.7	948	85	1.3	3252
07:44:16	22	913	80.0	4.0	928	83	1.4	3164
	22	914	79.7	3.7	928	86	1.3	3231
	27	912	79.3	4.0	917	86	1.3	3213
17.03.10	18	925	72.7	3.1	1202	87	1.5	2762
02:23:15	23	932	77.9	3.1	1088	85	1.5	3092
	18	926	77.4	3.1	1160	88	1.5	3151
	18	933	72.9	3.1	1352	89	1.6	2845
30.03.10	15	920	73.4	3.7	1051	85	1.5	2794
08:51:17	15	931	74.2	3.7	1202	87	1.5	2912
	15	922	78.1	3.7	1253	83	1.6	3096
	10	934	79.1	4.0	943	86	1.5	3280

In the case of quench heater path is not given to the application, no results are shown for the user either. Data from non-quench event on 10.04.08 at 21:30:22 is shown in Table 5.18. The heater firing time tFire appears much later than expected, so if this was a quench it would have had plenty of time to harm the circuit. Fortunately, this is not a quench and is only shown to make sure that analysis steps work properly.

Table 5.18 Quench Heater Voltage 10.04.08 at 21:30:22, No Quench

Heater Name	tFire / *ms*	Vinit_test / *V*
U_HDS_1	932	901
U_HDS_2	932	931
U_HDS_3	932	906
U_HDS_4	932	927

Figure 5.21 shows how the quench heater voltages behaved during this event.

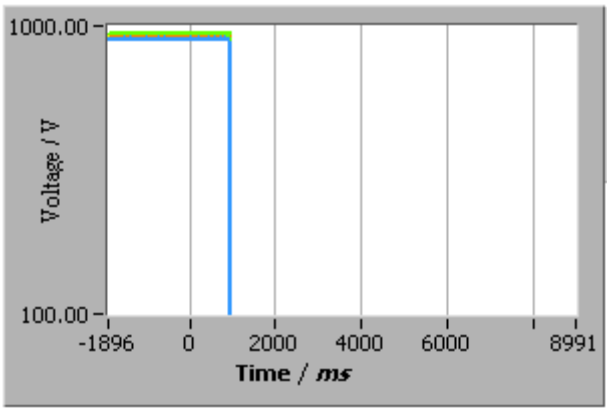

Figure 5.21 Quench Heater Voltage Graph 10.04.08 at 21:30:22, No Quench

It is clear, that the quench heater voltages did not behave the same way as they would if this was a quench event. Voltages drop to zero voltage sharply instead of discharging during a time interval.

5.6. Results for Time Delays

Time delay calculations are important in order to notice if all the triggers fired in time. Normal behavior of different triggers can be studied and in this way, differences in values do not remain unnoticed and may be a sign of malfunctions. Since trigger values differed more when comparing with more quenches, maximum, minimum and average values were determined using 36 different quench events instead of 12 quench events as seen with previous results. Values for detecting different trigger signals are shown in Table 5.19 for normal quenches. To remind, explanations for the signals are: quench detection time tD from U_QS0=100 *mV*, heater firing time tFire from U_HDS, trigger time tTrigger from I_REF=0 *A* and time tDump from U_DUMP_RES=100 *V*. They should appear in the order of tD < tFire (< tDump) < tTrigger and values are also shown in this order in the table from left to right. Voltage signal U_DUMP might be triggered at any time, and for this reason its values can vary and its appearance should not be analyzed. Basically tDump appears either before tTrigger or approximately at 400 *ms*, which is considered as a delayed opening. Any other times might be alarming and the application gives an alarm in these cases. There are always four tFire values in the measured values for four different heaters. Some tFire values for all the heaters have been shown in Table 5.16.

Table 5.19 Trigger Signal Times with 32 Normal Quench Events

	tD / *ms*	**tFire1 / *ms***	**1st tDump / *ms***	**tTrigger / *ms***
Max	-36.0	-7.3	427.07	0.010
Min	-72.4	-41.3	-19.07	0.000
Average	-54.0	-24.7		0.001

For symmetric quenches, values for detecting different trigger signals are shown in Table 5.20. Value for tFire is always taken with the same heater so that values for this heater are compared. Due to possible delayed quench detection, values for firing the quench heaters tFire are later than in the case of normal quenches. Some tFire values for all the heaters were already shown in Table 5.17.

Table 5.20 Time Delays for Symmetric Quenches

Date	**tD / *ms***	**tFire1 / *ms***	**1st tDump / *ms***	**tTrigger / *ms***
23.05.08 07:44:16	-14.1	22.1	-13	0
17.03.10 02:23:15	-8.22	17.7	-7	0
30.03.10 08:51:17	-21.5	14.8	-7	0
05.07.08 17:53	-10.0	10.7	-13	0

Again, if the path and signals for analysis are missing, user is notified of the missing signals and how it affects on the time difference calculations. Non-quench event from 10.04.08 at 21:30:22 gives alarming values, as shown in Table 5.21. These values are highlighted to the user in the actual application.

Table 5.21Time Delay for Non-quench Event

Date	**tD / *ms***	**tFire1 / *ms***	**1st tDump / *ms***	**tTrigger / *ms***
10.04.08 21:30:22	NaN	932	325	0

Table 5.22 shows time differences between trigger signals in the case of normal quenches. Differences are calculated so that dt1 is tFire-Td, dt2 is tDump-tFire, dt3 is tTrigger-tDump and dt4 is tTrigger-tFire.

Table 5.22 Time Differences for Normal Quenches

	dt1 / *ms*	**dt2 / *ms***	**dt3 / *ms***	**dt4 / *ms***
Max	41.5	345.7	19.0	36.2
Min	20.7	-5.7	-325.0	7.3
Average	30.4			23.7

From the results we can see that dt2 and dt3 values for normal values should not be compared since tDump times vary hugely because of varying triggering times.

Table 5.23 shows time differences between trigger signals in the case of symmetric quenches.

Table 5.23 Time Differences for Symmetric Quenches

Date	**dt1 / *ms***	**dt2 / *ms***	**dt3 / *ms***	**dt4 / *ms***
23.05.08 07:44:16	36.2	-35.1	13	-22.1
17.03.10 02:23:15	25.9	-24.7	7	-17.7
30.03.10 08:51:17	36.3	-21.8	7	-14.8
05.07.08 17:53	20.7	-23.7	13	-10.7

In this case dt2 and dt3 values for symmetric quenches can be compared since tDump was always triggered almost the same time.

6. DISCUSSION OF THE RESULTS

6.1. Discussion for Quench Detection

The application detects quench when U_QS0 reaches the limit of 100 *mV* and stays above the limit level for a certain time. However, quench has started before this and the application also approximates the time for this real quench Tq with the help of exchange rate from U_QS0. In the case of a symmetric quench, real quench time is taken in the same manner either from U_1 or U_2 depending on which one reached the threshold first. From the results we can see that threshold reach times and quench detection times are determined accurately.

Table 6.1 shows time differences between different quench detection times in the case of normal quenches. To calculate maximums, minimums and average values, 32 different quench events have been used.

Table 6.1 Normal Quenches: Detection Differences from 32 Quenches

	|Td-Tq| / *ms*	**|Tq_v-Tq| / *ms***	**U_QS0-U_1/U_2 / *ms***	**|U_1-U_2| / *ms***
Max	1026.3	11.1	-10.3	17.7
Min	5.2	0.0	-36.2	0.0
Average	47.8	1.3	-18.23	10.00

The maximum value for |Td-Tq|, that is between quench detection time Td and actual quench time Tq, is caused by a quench which is building up very slowly and this difference has a very high effect on the average value also. It takes a long time for this quench to reach its threshold after a quench begins. This quench has already been shown in Figure 4.7. Time differences between detected quench Td and real quench Tq give an idea how much the quench detection is delayed from the actual quench. Figure 6.1 shows |Td-Tq| difference results on 31 different quench events excluding the result from the slow quench.

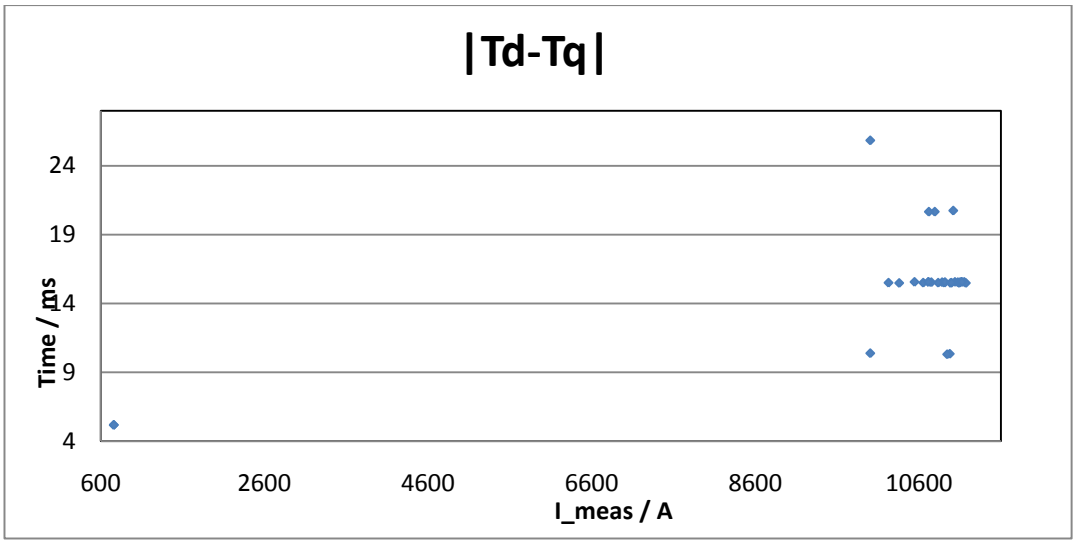

Figure 6.1 Normal Quench: |Td-Tq| in Milliseconds

From the graph points, it is seen that quench is normally detected about 16 *ms* after the actual quench beginning, but delays may be as low as 5 *ms* and as high as 1026 *ms*, as was the case of the quench that was building up slowly.

Figure 6.2 compares actual quench beginning times, as determined programmatically in Tq and by visually looking quench beginning Tq_v from the graph of U_QS0.

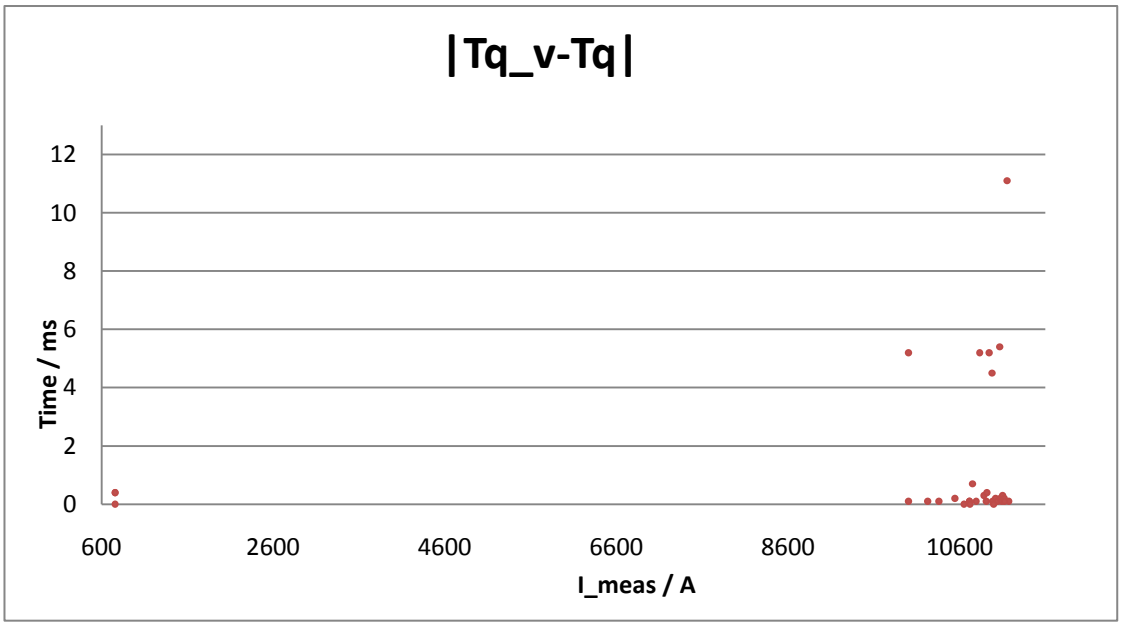

Figure 6.2 Normal Quench: |Tq_v-Tq| in Milliseconds

Most of the time, the application determines the values accurately. Some results vary by 5 *ms* which corresponds one point on the voltage graph. Once, actual quench time had a difference of 11.1 *ms* when comparing to the visual quench beginning. These small differences are due to actual quench beginning recognition algorithm. Algorithm

needs further designing to be more accurate. Variations around 0 *ms* are due to precision in application and small errors in determining the start time visually.

Figure 6.3 shows for normal quenches values between detecting U_QS0 to the detection of either U_1 or U_2.

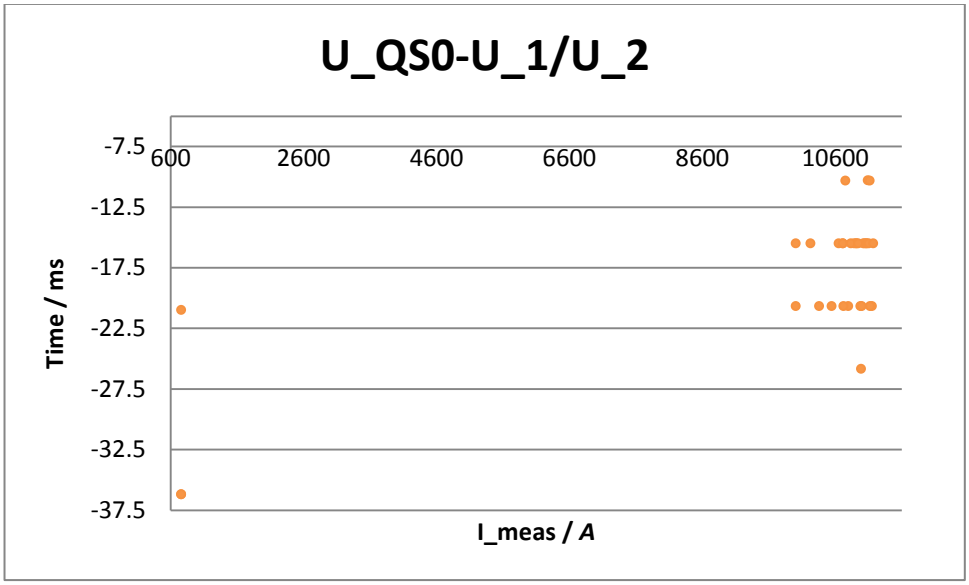

Figure 6.3 Normal Quench: U_QS0-U_1/U_2 in Milliseconds

These results can be used as proof that observing changes in voltage differences between U_1 and U_2 is essential for safe quench detection. U_QS0 detects voltage changes and reaches its threshold by average 18 *ms* before it would be detected by observing only U_1 and U_2. The biggest difference between detection times is 36 *ms*, during which a quench would have plenty of time to wreck the magnets and the LHC circuit.

Figure 6.4 shows when the quench reaches the second aperture.

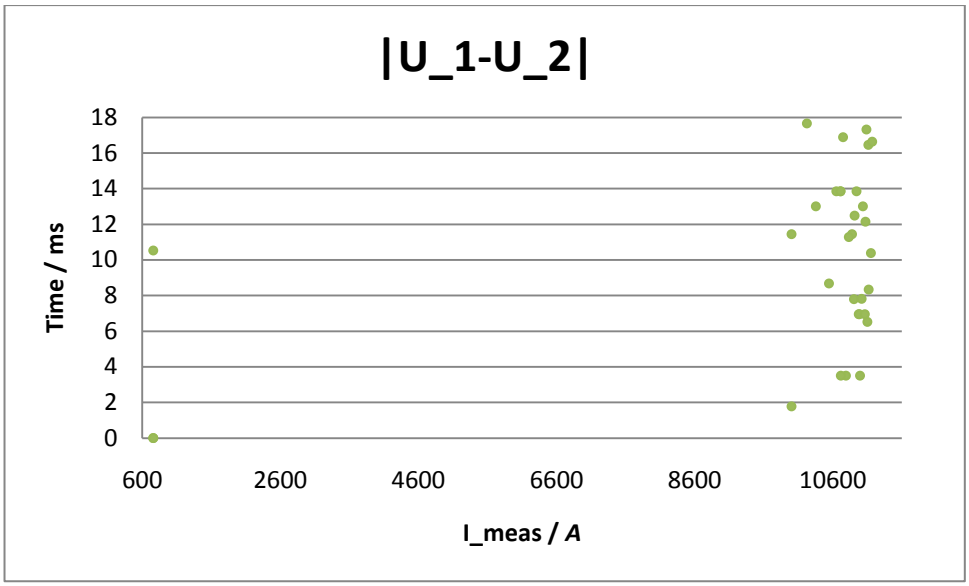

Figure 6.4 Normal Quench: |U_1-U_2| in Milliseconds

It is seen that a quench reaching second aperture might happen anywhere between 0 and 18 *ms* according to the data studied. In addition, for all these results, there is no visible difference between low and high currents.

Furthermore, actual quench beginning times are studied for symmetric quenches and results are shown in Table 6.2.

Table 6.2 Symmetric Quenches: Detection Differences

	|Td- Tq| / *ms*	**|Tq_v-Tq| / *ms***
Max	5.6	0.0
Min	2.6	0.0
Average	4.2	0.0

Time difference between quench and its detection for symmetric quenches is between 2 and 6 *ms.* Actual quench time Tq and quench detection time Td in the case of symmetric quench appear closer to each other. The reason for this is probably due to the fact that voltages change quicker in the case of symmetric quenches and U_1 and U_2 also reach their threshold quicker. No difference in actual quench times was observed for symmetrical quench events which were studied. However, only four different events were studied for this purpose and further studying might reveal some differences.

Quench detection with U_QS0 fastens the detection of quench but only within the set threshold limits. For this reason, the user still has the responsibility to check that values given by the application are correct by manually checking the graphs and firing time of the triggers. The application helps the work by automatically checking some parameters and alarming levels but does not replace the need for operators to check the values. However, it does fasten the analysis time since checking of the values can be done reasonably fast.

6.2. Discussion for Quench Energy

Values for MIITs, field and stored energy are completely dependent on the value of current. Field and stored energy graphs are linear and the value of MIITs is based on an interpolation made with 10 different values from a current. Since MIITs value is calculated based only on the highest value the current reached, it should not be trusted completely. The amount of values used for the interpolation function could be increased to get better results. Interpolation functions for both dipole and quadrupole have been implemented, but only the dipole quenches are recognized so far. If needed to recognize quadrupole quenches, the code needs modifying.

As the results are shown on date order and the first eight quenches in Table 5.14 are training quenches, gradual improvement of the quench current can be seen. In the beginning magnet quenches at 10651 *A*, and after training 11123 *A* is accomplished. Figure 5.15 shows that values build up linearly as expected. Small errors in results are due to precision used for showing of the results in the application.

MIITs model for quadrupole has been created but in this phase of the application, it is most important that the dipole analysis works well. Quadrupole quenches are quite rare and are mostly induced by beam losses. Beam loss monitoring system has been designed at CERN and beams are dumped if beam loss goes above a predefined threshold. In theory beam losses should not happen. However, in the event of for example power supply failure, they might occur. Quadrupole MIITs calculation has been added to the code for later use when application is extended for quadrupole quenches.

6.3. Discussion for Quench Location

By comparing the results from quench detection and quench location, it is seen that every time U_2 reaches threshold before U_1, location is internal as expected. Vice versa, when U_1 reaches threshold before U_2, location is external. In the case of symmetric quench, quench location turns out to give additional information than quench location time. Time difference between U_1 and U_2 reaching the threshold is sometimes so small that it is not seen in Td for reasons of shown precision. However, comparing the values programmatically detects the difference, and this difference is seen in location. If signals change simultaneously without difference, quench location of Ext/ Int is given.

At the moment, application only gives information on which aperture the quench started from. Previous version for SM18 gave information on dipole, pole, layer and section. In the tunnel conditions, however, not as many signals are measured. This gives user less information on quench location.

6.4. Discussion for Quench Heaters

Since quench heater voltages in the tunnel are different from the heaters used in SM18, quench heater alert levels had to be determined again. With the help from the data collected with the new application, expected alarm levels for the new application could be determined. In the case of normal quenches, maximum, minimum and average values for quench heaters have been calculated with 32 different quench events and results are shown in Table 6.3.

Table 6.3 Values from 32 Quench Events

	tFire / *ms*	**Vinit_test / *V***	**Imax / *A***	**Vmin / *V***	**tminV / *ms***	**TauIniV**	**Tau JmpV**	**E / *J***
Max	-21.0	936.0	82.0	4.9	1600.0	101.0	2.0	3678.0
Min	-33.0	901.0	69.6	2.8	787.0	76.0	0.8	2290.0
Aver	-24.7	917.0	77.2	3.7	1061.2	87.2	1.2	3103.7

Some of these values varied highly on previous SM18 results and alarm levels. Alarm levels for the previous application are shown in Table 6.4.

Table 6.4 Previous Alarm Levels for Quench Heaters

	tFire / *ms*	**Vinit_test / *V***	**Imax / *A***	**Vmin / *V***	**tminV / *ms***	**TauIniV**	**Tau JmpV**	**E / *J***
Max	6	920	Inf	15	600	117	6	3000
Min	-2000	810	0	0	380	60	-6	2000

In addition, example of SM18 measurement results is given in Table 6.5 to help in comparison between previous and new measurement results.

Table 6.5 Previous Measurement Results for Different Heaters

	tFire / *ms*	**Vinit_test / *V***	**Imax / *A***	**Vmin / *V***	**tminV / *ms***	**TauIniV**	**Tau JmpV**	**E / *J***
QH1	2	835	69.5	4.4	457	81	1.4	2339
QH2	2	830	69.3	4.0	481	75	1.4	2163
QH3	2	836	69.8	5.2	502	80	1.5	2387
QH4	2	854	70.3	6.4	442	77	1.4	2311

With SM18 data and previous alarm levels, the user is not notified of any alarming levels. However, if these alarm levels were to be used for the new data, various alarms would be shown incorrectly for the new measurement data.

In the case of tFire lower time limit could be kept as low as -2000 *ms* since it is not so alarming if the heaters fire early. Problems appear if they fire too late since then the quench might not propagate fast enough. Higher limit has been set to 6 *ms* which is too late related to the data trigger time at 0 *ms*. Heater firing time tFire should appear at least before that time. Test results from Vinit_test show that the average value for initial voltage is already as high as 917.0 *V*. Upper limit on alarm values have been set to 920 *V* which appears to be too low and gives alarms for normal values. Imax alarm levels can be kept the same as there was no set higher limit and results are in the same order of magnitude. Vmin upper limit is set to 15 *V*. This seems rather high, if we look at the results from the measurements. Limits for time for minimum voltage tminV had been set to be between 380 *ms* and 600 *ms*. It is not quite clear, what had been done in the existing application to calculate tminV. It seems tminV was actually tminV-tFire but even with this calculation, the results in the table did not seem right. For example, tminV appeared at the point of 900 *ms* and tFire of 2 *ms* was deducted from this. The table for the previous application was showing the result for this to be 457 *ms* and it could not be determined where this value came from. The new application is now calculating the actual tminV-tFire, and for this reason, values for the alarms needed to be changed. All the results from the measured values appear between 787 and 1600 *ms* and this leaves both of the set limits way too low. TauIniV are also higher with the new measurement data compared to the previous data. Alarm limits have been quite high (117 *V)*, when the highest value for the new measurement data is known to be 101 *V*. With these existing limits, the measured average lies almost exactly in the middle, so these limits may be considered good. TauJmpV limits appear to be also very close to the limits which the new measurement data. Due to the fact of lower heater voltages being used in SM18, limits for energy E have also been set quite low for the previous measurement data. Higher limit has been set to 3000 *J* although with the new data, values as high as 3678 *J* are present. Even the average value for energy lies higher than 3000 *J*. Lowest measured value for new data is already as high as 2290 *J*.

There is no huge difference between the maximum and minimum values between normal and symmetric quenches as shown in Table 6.6. The only thing which really changes is the time of firing the heaters tFire, but this of course is due to the delayed quench detection.

Table 6.6 Symmetric Quench: Maximums and Minimums

	tFire / *ms*	**Vinit_test / *V***	**Imax / *A***	**Vmin / *V***	**tminV / *ms***	**TauIniV**	**TauJmpV**	**E / *J***
Max	27	934	80.4	4.3	1543	89	1.6	3280
Min	10	910	72.7	3.1	839	83	1.0	2722

New alarm limit levels can be set according to the data studied and proposal for new limits can be seen in Table 6.7.

Table 6.7 New Alarm Levels for Quench Heaters

	tFire / *ms*	**Vinit_test / *V***	**Imax / *A***	**Vmin / *V***	**tminV / *ms***	**TauIniV**	**Tau JmpV**	**E / *J***
Max	0	1001	Inf	15	1610	117	6	3680
Min	-2000	819	0	0	780	64	-6	2280

From the results given by the quench heater analysis, the user can notice if heaters are not working properly and if it would be time to change them. Even so, if some of the heaters are not working properly, magnets are still safe and protected since the heater design has taken this into account by not relaying on the proper firing of all the heaters.

6.5. Discussion for Time Delays

Table 5.19 showed maximum, minimum and average results, in the case of normal quenches. It is noticed that tD appears normally between -72 and -36 *ms*, tFire between -41.3 and -7.3 *ms*, tDump has differences as expected and tTrigger is always expected to appear at 0 since time for X=0 has been determined from tTrigger. Figure 6.5 shows trigger times from all quench events used to gather the data.

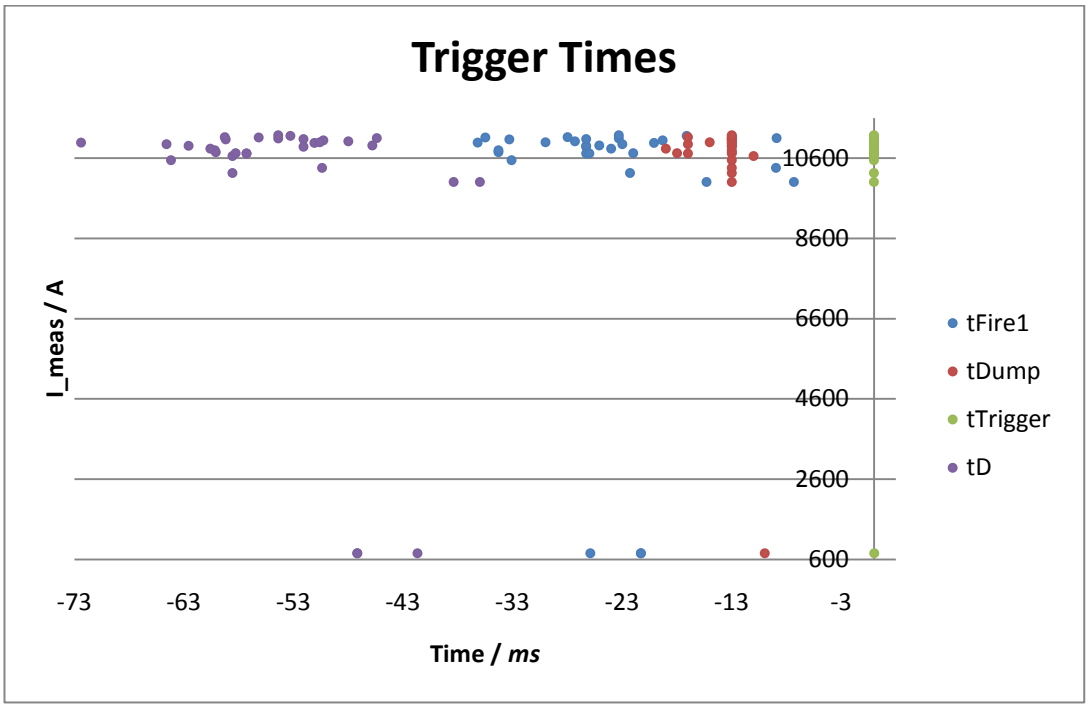

Figure 6.5 Normal Quenches:Trigger Times

In the case of symmetric quenches, all the detection times tD for U_QS0 reaching the threshold are delayed. In addition, tFire is fired later also because its functioning is related to detection of the quench. Maximum, minimum and average values are shown in Table 6.8.

Table 6.8 Time Delays for Symmetric Quenches

	tD / *ms*	**tFire1 / *ms***	**1st tDump / *ms***	**tTrigger / *ms***
Max	-8.2	27.0	-2.0	0.0
Min	-21.5	9.6	-13.0	0.0
Average	-13.5	16.6	-8.4	0.0

Time tD appears between -21.5 and -8.2 *ms*, tFire between 9.6 and 27 *ms*, tDump between -13.0 and -2.0 *ms* and tTrigger at 0.0 *ms*.

In the case of normal quenches, time difference dt1 is between 20.7 to 41.5 *ms*. Time differences dt2 and dt3 have maximum and minimum values which vary a lot because of the difference in the value of tDump firing. Time difference dt4 is between 7.3 to 36.2 *ms*.

Maximum and minimum differences for different events in the case of symmetric quenches are shown in Table 6.9.

Table 6.9 Time Differences for Symmetric Quenches

	dt1 / *ms*	**dt2 / *ms***	**dt3 / *ms***	**dt4 / *ms***
Max	36.3	-21.8	13.0	-10.7
Min	20.7	-35.1	7.0	-22.1

Time difference dt1 is between 20.7 and 36.3 *ms*. This is similar values as with the normal quenches. Time difference dt2 is between -35.1 and -21.8 *ms*. These values differ from normal quench values and can serve as a sign of abnormal quench. Time difference dt3 is between 7 and 13 *ms* and time difference dt4 is between -22.1 and -10.7 *ms*. From these dt4 has abnormal values and could serve as an alarming sign to detect abnormal quench.

6.6. Discussion for Error Sources

Considering possible error sources for the results, we have to take into account of course, measurement errors caused by the LHC detection and measurement tools. In addition, mathematical models are never perfect even with a good algorithm. One could think that the used algorithms in the application are too simple or non-flexible and in this way wrong or inaccurate results appear. Some differences might also appear during

different analysis steps, when measurement data is cut and there might appear some differences. It has also been noticed that during the design and on the final results rounding and precision gives errors. X-axel differences are also possible since 0 point had to be determined differently for different buffers. Apparently, small differences between specification of time from QPS and FGC file buffers exist also.

7. CONCLUSIONS

The goal of this thesis was to study the physics phenomena of superconductivity and especially quench. In addition, it described how the existing LHC magnet quench analysis was extended to the new Quench Protection System data.

The work began with theory on superconductivity, quench and quench protection. After that, methods used to meet the goal in designing a new application for quench analysis were discussed. With the help of this new analysis tool, it was possible to gain results such as quench time, location, energy, quench heater operation and time differences between different triggers. Different analyses are done automatically to save time for more important activities and thus reducing the time needed for data analyzing and inactive mode of the LHC.

By looking at the targets which were set in the beginning of the project, the application did not manage to fulfill all the requirements. However, all the basic information about the quench event, which was the main part of the project, is delivered and analyzed by the application. Anyhow, the ability to analyze multiple quenches and their propagation was not implemented in the application. In addition, the application is designed to analyze the quench of dipoles which includes most of the quench events. In the future, analyzing quadrupole quenches should be implemented. Very little feedback on the new application from the users was received and no improvement could be made based on this data. Ideas to improve the user interface and usability would have been useful.

At the end section of the thesis, values from different quench analyses were examined. Based on these tested quench events, the application behaves and gives reliable results, but further observing with various quench events is necessary. New alarm limits could be set according to observations on values for various analysis steps. Further improvement of the application would include code performance checking, such as memory usage and execution time optimizing.

It is important to notice that the new application for quench analysis enables to analyze quench automatically from the SDDS-files and from the user point of view usability of the application has improved. For example, units, signal names and explanations were added to the graphs where needed and general appearance of the user panels improved. Additional alarms were added and all the alarm and threshold values were relocated to files or global variables to be easily found in case they need to be changed later on. The new application becomes especially useful in the year 2011 when the LHC is switched for even higher energies and more quench events can be expected.

It was later found, that the original version of the application was still needed for SM18 after their software and hardware renovation. However, implementing both new and previous version of AQA to use same application version, might include huge amount of changes to be made to the code. It was decided to use the original version with some cosmetic changes since this was found to be quicker solution at that moment. In the future, combining these two versions should be done to reduce the time needed for changes to the cosmetics of the user interface.

Based on different AQA versions, different analysis tools have been created for different needs and users. This brings difficulties when new versions need to be released for new or different LabVIEW or Linux versions, since the user panels differ from the previous ones. From the point of view of the designer, all of these applications have to be renewed independently. Some of these applications could be combined so that same application could be used for different analyses. The basic concept of the designed application could be used to analyze quench events in different experiments such as in the case of biomedical superconductive magnets. However, limitations of use for different magnet analyses include use of SDDS -file format, configuration file settings and setting of the threshold values. Limits and configurations need further designing since different information and signals would be available.

When it comes to the LHC, it has already proven to be able to reveal new physics phenomena and who knows what it exposes in the future. CERN continues to stimulate new innovations and pilot applications for medical and other fields now and in the future. In general, research of superconductivity for new materials, especially in room temperature conditions, contribute to the application possibilities and have the potential to bring superconducting devices into our every-day lives. Superconductivity has also the ability to help in climate protection as less material is needed for device construction. In addition, reduction in power losses saves electricity and leads to lower greenhouse gas emissions. This however is associated with the uncovering of some new superconducting materials and more investments in new superconductive technologies. [Hartikainen 2005]

REFERENCES

Allison, J., MRI Safety. [Presentation]. [Cited 25.11.10]. Available: http://www.radiology.mcg.edu/RadiologyPhysics/mri/MRI%20Safety7_very_short_form.ppt.

Andreassen, O. 2009. Post Mortem for the LHC. [Presentation]. CERN.

Bhunia, U. 2003. Cryogenics for LHC Dipole. CERN-India Collaborator, Department of Atomic Energy, VECC, Kolkata, India. [Article]. 27.11.03.

CAS 1996. Superconductivity in particle accelerators. CERN Accelerator School. [Lecture proceedings from Hamburg, Germany, 17.-24.05.95]. Editor: S. Turner, Geneva. Page count 361.

CERN European Organization for Nuclear Research [WWW]. [Cited 25.08.10]. Available: http://public.web.cern.ch/public/en/LHC/LHC-en.html.

Clarke, J., Hatridge, M. and Mößle, M. 2007. SQUID-Detected Magnetic Resonance Imaging in Microtesla Fields. Department of Physics, University of California, Berkeley, California. [Article].

CMS Compact Muon Solenoid Experiment 2010. First Z bosons detected by CMS in heavy-ion collisions. [WWW]. [Cited 19.11.10]. Available: http://cms.web.cern.ch/cms/News/2010/FirstZs-HeavyIons/index.html.

Conectus Consortium of European Companies determined to use superconductivity [WWW]. December 2009. [Cited 30.08.10]. Available: http://www.conectus.org/market.html.

Della Corte, A. 2009. Superconductivity. The Frascati Research Centre of ENEA, Italy. [Document]. January 2009.

Erokhin, A. 2008. Main dipoles MB. CERN. [Document]. 30.01.08.

EuH European Hospital Verlags GmbH 2009. 11.7-T scanner a magnet to draw international researchers to France. [Article]. 11.12.09.

Ferracin, P., Prestemon, S. and Todesco, E. 2009. Superconducting Accelerator Magnets. [Lecture slides from US Particle Accelerator School]. [Cited 10.08.10]. Available: http://thunder.lbl.gov/PFerracin/USPAS/USPAS_Albuquerque_0609.html.

FYS-1500 Kiinteän olomuodon fysiikka C. 2010. Tampere University of Technology. [Moodle -course material]. [Cited 09.08.10]. Available: moodle.tut.fi.

GE General Electric Healthcare [WWW]. [Cited 27.08.10]. Available: http://www.gehealthcare.com.

Gourlay, S.A. 2008. Challenges and Prospects for the Large-Scale Application of Superconductivity. [Article in IEEE Transactions on Applied Superconductivity, Vol. 18, No. 3, September 2008].

Hartikainen, T. 2005. Environmental Impacts of Superconducting Power Applications, Tampere University of Technology. Finland [Doctoral thesis].

Hitachi Medical Systems [WWW]. [Cited 27.08.10]. Available: http://www.hitachi-medical-systems.eu.

Jokela, K., Korpinen, L., Hietanen, M., Puranen, L., Huurto, L., Pättikangas, H., Toivo, T., Sihvonen, A-P. and Nyberg, H. 2009. Sähkömagneettiset kentät: Säteilylähteet ja altistuminen: Chapter 9.10 Magneettikuvauslaitteet. [STUK book series]. Available: www.stuk.fi.

Kurfuerst, C. 2010. Personal discussions.

LANL Los Alamos National Laboratory [WWW]. Biomedical developments. [Cited 31.08.10]. Available: http://www.lanl.gov/orgs/mpa/stc/biodev.shtml.

Lvovsky Y. and Jarvis, P. 2005. Superconducting Systems for MRI -Present Solutions and New Trends. [Article in IEEE Transactions on Applied Superconductivity, Vol. 15, No. 2, June 2005].

Magnet Lab National High Magnetic Field Laboratory 2010. Florida State University, Los Alamos National Laboratory, University of Florida. [WWW]. [Cited 27.08.10]. Available: http://www.magnet.fsu.edu/.

McDermott, R., Lee, SK., ten Haken, B., Trabesinger, A.H., Pines, A. and Clarke, J. 2004. Microtesla MRI with a superconducting quantum interference device. Materials Sciences Division, Lawrence Berkeley National Laboratory. [Article]. 24.05.04.

Mess, K-H., Schmuser, P. and Wolff, S. 1996. Superconducting Accelerator Magnets. Singapore: World Scientific. 218 p.

Motiwala, P. D. and Sridhar, S. Superconductivity and basics understanding of magnet testing in SM18. CERN. [Document].

PostM Post Mortem [WWW], [Cited 02.12.10] Available: http://proj-lhc-software-analysis.web.cern.ch/proj-lhc-software-analysis/analysis/post_mortem.htm.

PR15 Press release of CERN 2010. ICHEP 2010 conference highlights first results from the LHC. [Cited 20.08.10]. Available: http://press.web.cern.ch/press/PressReleases/Releases2010/PR15.10E.html.

Quench-analysis. CERN, Node34. [Document].

Rijllart, A., Khomenko, B., Kudriavtsev, D., Raimondo, A., Reymond, H., Trofimov, N. 2007. The First Stage of the Post Mortem Analysis Software Used for the Hardware Commissioning of the LHC. CERN, Geneva, Switzerland. [Proceedings of ICALEPCS07].

Rodriguez-Mateos, F., Pugnat, P., Sanfilippo, S., Schmidt, R., Siemko, A. and Sonnemann, F. 2000. Quench Heater Experiments on the LHC Main Superconducting Magnets. [Article].

Rodriguez-Mateos, F. Sonnemann, F. 2001. Quench heater studies for the LHC magnets. [Proceedings of the 2001 Particle Accelerator Conference, Chicago].

Rossi, L. 2009. Superconductivity: its role, its success and its setback in the Large Hadron Collider (LHC) of CERN. [Article in Superconductor Science and Technology, Volume 23, No.3, March 2010].

Rottier, R. 2000. The application of Superconductors in Medicine. [Article]. 20.09.00.

Servomaa, A. and Parviainen, T. 2001. STUK-A184 Säteilyturvallisuus ja laatu röntgendiagnostiikassa (Radiation Safety and Quality in Xray Diagnostics). STUK Finnish radiation and nuclear safety authority. [Report]. May 2001.

Siemens Medical [WWW]. [Cited 27.08.10]. Available: http://www.medical.siemens.com.

Siemko, A. 2001. Magnet Quench Process. CERN, Geneva, Switzerland, Chamonix, France. [Document]. 15. – 19.01.01.

SM18. Quench Analysis. CERN. [Document].

Superconductors.org [WWW] 2010. [Cited 06.08.10]. Available: http://www.superconductors.org/.

Varian Inc [WWW]. [Cited 27.08.10]. Available: http://www.varianinc.com.

Verweij, A., Baggiolini, V., Ballarino, A., Bellesia, B., Bordry, F., Cantone, A., Casas Lino, M., Castaneda Serra, A., Castillo Trello, C., Catalan Lasheras, N., Charifoulline, Z., Coelingh, G., Dahlerup-Petersen, K., D'Angelo, G., Denz, R., Feher, S., Flora, R., Gruwe, M., Kain, V., Khomenko, B., Kirby, G., MacPherson, A., Marqueta Barbero, A., Mess, K.-H., Modena, M., Mompo, R., Montabonnet, V., le Naour, S., Nisbet, D., Parma, V., Pojer, M., Ponce, L., Raimondo, A., Redaelli, S., Reymond, H., Richter, D., de Rijk, G., Rijllart, A., Romera Ramirez, I., Saban, R., Sanfilippo, S., Schmidt, R., Siemko, A., Solfaroli Camillocci, M., Thurel, Y., Thiessen, H., Venturini Delsolaro, W., Vergara Fernandez, A., Wolf, R. and Zerlauth, M. 2008. Performance of the main dipole magnet circuits of the LHC during commissioning. CERN, Geneva, Switzerland. [Article, proceedings of EPAC08, Genoa, Italy].

Wilson, M. N. 1983. Superconducting Magnets. Oxford: Clarendon Press, (Repr. 2002). 335 p. (Mono. Cryog. ; 2).

Wired.com Daily technology news. Most Powerful MRI Has Stronger Magnet Than the LHC's. [WWW]. 16.09.09. [Cited 27.8.2010]. Available: http://www.wired.com/wiredscience/2009/09/bigmri/.

Yurkewicz, K. 2007. Protecting the LHC from itself. [Article in Symmetry -particle physics magazine published by Fermi National Accelerator Laboratory and SLAC National Accelerator Laboratory, Vol. 4, December -07].